

TDK Thesis

Rhiannon Nohealani Rodgers
2023

University of Veterinary Medicine Budapest
Department of Microbiology and Infectious Diseases



**Modification of the Innate Immune Response using Low
Molecular Weight Substances and its Effects on Renal
Carcinoma Cells in a Mouse Model**

Rhiannon Nohealani Rodgers

Supervisors:

Gulyás Dominik Ádám, Departmental Engineer
Department of Microbiology and Infectious Diseases
University of Veterinary Medicine Budapest

Dr. Lőrincz Márta PhD, Senior Lecturer
Department of Microbiology and Infectious Diseases
University of Veterinary Medicine Budapest

Budapest, Hungary

2023

Table of Contents

1. Introduction	3
1.1. OX40 and Anti-OX40	7
1.2. Cytosine-Phosphorothioate-Guanine	9
1.3. CpG and Anti-OX40	10
1.4. Retinoic Acid-Inducible Gene I	11
1.5. IL10, IL6, and IFN γ	12
1.6 The RENCA CRL-2947 Cell Line	15
2. Aims	17
3. Materials and Methods	17
3.1. Cancer Cell Line	17
3.2. Dosages and Course of Treatment	18
3.3. Cell Pre-Experiment	19
3.4. Measurement of Cytokine Production	19
3.5. Postmortem Data Collection	20
3.6. Post-Experiment	21
3.7 Data Analysis	21
4. Results	22
4.1. Assessment of Median Survival Times	22
4.2. Primary Tumor Growth	23
4.3. Cytokine ELISA Tests	24
4.4. Reduction of Metastases	26
5. Discussion	29
6. Abstracts	32
6.1 English Abstract	32
6.2 Hungarian Abstract	33
7. Reference List	35
8. Figures List	38
9. Acknowledgements	40

List of Abbreviations

3p-hpRNA – Triphosphate Hairpin RNA

Ab – Antibody

APC – Antigen Presenting Cell

BATF – Basic Leucine Zipper ATF-Like Transcription Factor

BSF-2 – B-cell Stimulating Factor 2

CAR – Chimeric Antigen Receptor

CARD – Caspase Active Recruitment Domain

CD – Cluster of Differentiation

CpG – Cytosine-phosphorothioate-Guanine

CTLA-4 – Cytotoxic T-Lymphocyte-Associated Protein 4

DNA – Deoxyribonucleic Acid

dsRNA – Double-stranded Ribonucleic Acid

ELISA – Enzyme-Linked Immunosorbent Assay

FOXP3 – Forkhead Box P3

HGF – Hybridoma Growth Factor

HSF – Hepatocyte Stimulating Factor

ICB – Immune Checkpoint Blocker

IFN – Interferon

IKK ϵ – Inhibitor of NF- κ B Kinase ϵ

IL – Interleukin

IL-6R – Interleukin-6 Receptor

IRF – Interferon Regulatory Factor

ISG – Interferon Stimulated Gene

JAK – Janus Kinase

Kbp – Kilo-base pair

LGP2 – Laboratory of Genetics and Physiology 2

MDA5 – Melanoma Differentiation-Associated 5

MHC – Major Histocompatibility Complex

mRNA – Messenger Ribonucleic Acid

NF- κ B – Nuclear Factor Kappa-light-chain-enhancer of activated B cells

NK – Natural Killer

ODN – Oligodeoxynucleotide

OX40L – OX40 Ligand

PAMP – Pathogen-Associated Molecular Pattern

PBS – Phosphate-Buffered Saline

PD-1 – Programmed cell Death protein 1

PRR – Pattern Recognition Receptor

RIG-I – Retinoic Acid-Inducible Gene I

RLH – RIG-Like Helicases

RLR – RIG-I-Like Receptor

RNA – Ribonucleic Acid

RPMI – Roswell Park Memorial Institute

ssRNA – Single-stranded Ribonucleic Acid

STAT – Signal Transducer and Activator of Transcription

TSA – Tumor Specific Antigen

Teffs – Effector T-cells

TGF β – Transforming growth factor- β

Th – T-Helper cells

TLR – Toll-Like Receptor

TNF α – Tumor Necrosis Factor α

TNFR – Tumor Necrosis Factor Receptor

TNK1 - Thirty-eight Negative Kinase 1

TRAF3 – Tumor Necrosis Factor Receptor-Associated Factor 3

Tregs – Regulatory T-cell

1. Introduction

In the case of spontaneous neoplasias, the host immune system has a series of natural defenses to prevent further replication of damaged cells. However, in a process known as immune evasion, a growing tumor can inactivate the present T-lymphocytes, or T-cells, resulting in a relatively unimpeded ability to replicate and expand. The objective of immunotherapy within the sphere of current oncotherapies is to reactivate the immune system to allow eradication of the tumor without undesirable side effects. Each other sphere of oncotherapy—including, but not limited to radiotherapy, chemotherapy, and surgical excision— have their own benefits and drawbacks. Immunotherapy itself is generally split into four main categories: Immune checkpoint blockers (ICBs), cancer vaccines, cytokine therapies, and chimeric antigen receptor (CAR) T-cells [1]. As shown in **Figure 1-1**, each category has its own set of shortcomings, but the current frontiers of immunotherapy research are uncovering new ways to circumvent these drawbacks.

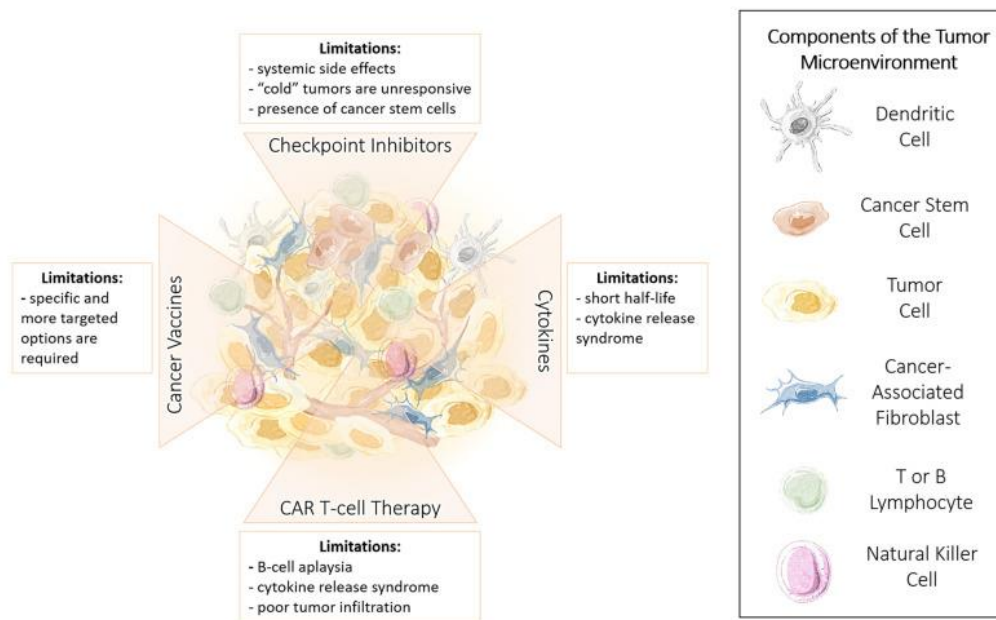


Figure 1-1: Showcasing the four categories of immunotherapy. From left to right: Cancer Vaccines, Checkpoint Inhibitors (ICBs), Chimeric antigen receptor (CAR) T-cell therapy, and Cytokines [1].

Thorough knowledge of the pathway with which the body first recognizes a tumor, and subsequently how a tumor can deactivate the regular expression and activity of T-cells, is required to understand where and how to select a target for therapy.

The process of immune activation begins when altered cells release tumor-specific antigens (TSA) that are exclusive to a present tumor. Antigen-presenting cells (APC), such as dendritic cells, will present these TSAs on their surface membrane using major histocompatibility complexes (MHC), notably MHC-I and MHC-II, which help T-cells identify the TSAs [2]. Once the tumor antigens have been presented, the T-cells still need an intermediary step in order to activate. This step comes in the form of CD80 and CD86 co-ligands, as well as a CD28 receptor [3–5]. These CD80/86 signaling ligands are likewise presented on the surface of mature APCs and will bind to CD28, which is found on the surface of undifferentiated T-cells [6]. This CD80/86/28 polymer transduces a vital signal required for T-cell activation. Alongside this pathway, members of the tumor necrosis factor receptor (TNFR) superfamily are also essential co-stimulators in T-cell activation, which will be further discussed in section 1.1 [7].

Once activated, these T-cells differentiate into effector T-cells (Teffs), which include cytotoxic CD8⁺ T-cells, and helper CD4⁺ T-cells. Activated CD8⁺ cells then proceed to target any altered cells presenting the recognized TSA and induce cell death using cytotoxic molecules such as tumor necrosis factor α (TNF α) and interferon (IFN)- γ [8]. Effector CD4⁺ T-cells, on the other hand, are critical both in forming long-term memory CD8⁺ cells [3, 9–11], as well as in licensing dendritic cells to express higher amounts of MHCs and releasing chemokines, which in turn activate more CD8⁺ cells and prolong their survival [3, 12]. CD4⁺ T-cells can also further be categorized into T-helper (Th) 1 and Th2 cells. Th1 cells produce cytokines like IFN γ and interleukin (IL)-2, which activate cell-mediated immune processes. Th2 cells produce cytokines IL-4, IL-5, IL-10, and IL-13, whose mechanism of action is associated with B-cell activation and other humoral immune responses [13, 14]. These differentiations can be seen simplified in **Figure 1-2** [15].

By activating these innate immune-signaling pathways alongside immunomodulatory cytokines, the body should efficiently eradicate neoplastic cells. If these pathways could always continue unimpeded, oncology would not need to exist. However, in addition to TSAs, tumor cells release immunosuppressive cytokines like transforming growth factor- β (TGF- β) and IL-10, both of which have potent anti-inflammatory properties [16].

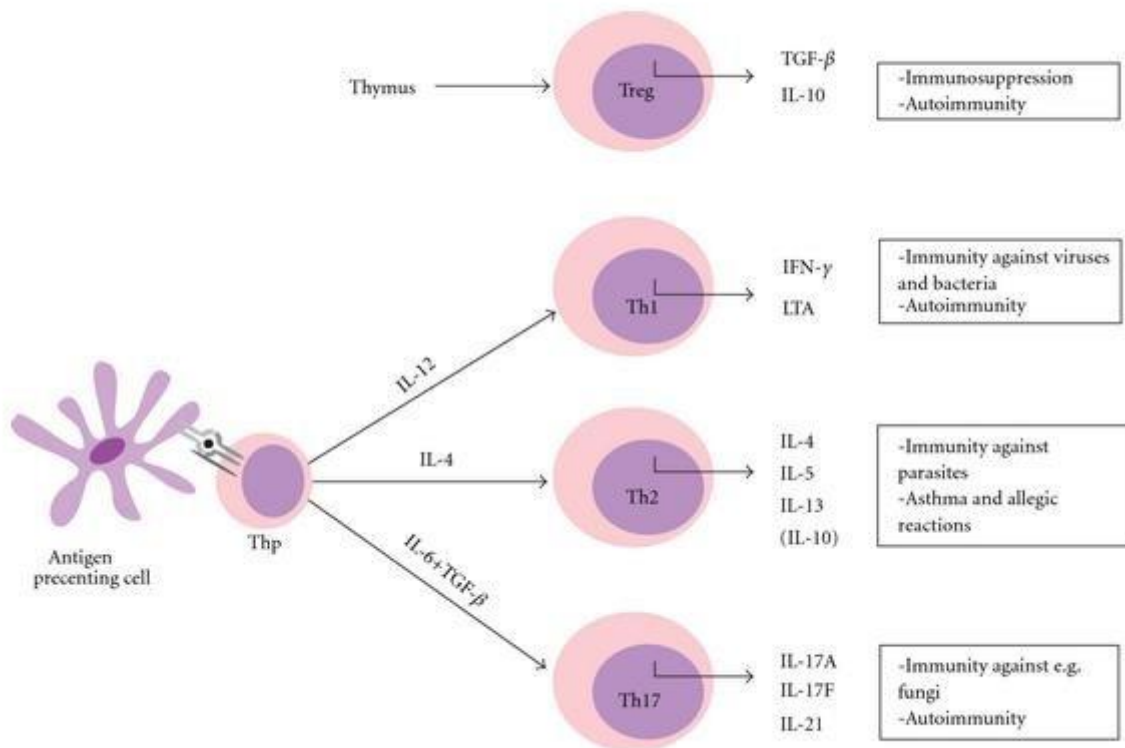


Figure 1-2: A visual representation of various sub-groups found in differentiated T-cells. **Thp** – Naïve T-cells. **IL** – Interleukin. **TGF-β** – Transforming Growth Factor Beta. **Th1** – Type 1 helper T-cell. **Th2** – Type 2 helper T-cell. **Th17** – Type 17 Helper T-cell. **Treg** – Regulatory T-cell [15].

The former, TGF-β, typically acts as a checkpoint for immune cells along barrier tissues, preventing unwarranted tissue damage during homeostasis, as it helps autoreactive T-cells maintain tolerance to environmental antigens [17, 18]. It does this by acting directly on promoting the expansion of regulatory T-cells (Tregs), which are responsible for counterbalancing reactive, proinflammatory Tefs. These Tregs are formed when naïve CD4+ T-cells are exposed to TGF-β, which induces the expression of Forkhead box P3 (FOXP3), a key gene in Tregs differentiation [14, 15]. TGF-β also conversely downregulates the generation and activity of Tefs, natural killer (NK) cells, and even APCs, resulting in a suppressed inflammatory response overall [18]. IL-10 shares many functional similarities with TGF-β; however, their primary distinction lies in their respective roles in immune regulation. TGF-β exhibits a more context-dependent and nuanced role, while IL-10 primarily acts as a type II/anti-inflammatory cytokine, which controls inflammation near infections to prevent harmful escalation [18, 19].

In the context of cancer, however, their roles are very similar. In the early stages of cancer development, both IL-10 and TGF-β limit the potential secondary damage to healthy

surrounding tissue caused by tumor-induced proinflammatory cytokines. However, in later stages, many neoplastic cell strains can exploit TGF- β and IL-10 to inactivate NK and T-cells, allowing a more complete immunosuppression in the microenvironment [20]. They achieve this by preventing APCs from producing a greater number of proinflammatory cytokines, such as IL-12 [19, 21, 22].

Furthermore, neoplastic cells in the tumor microenvironment express immune checkpoint molecules, such as programmed cell death protein (PD-1) and cytotoxic T-lymphocyte-associated protein 4 (CTLA-4), that counteract antigen receptor signaling and produce immunosuppressive effects [7, 20]. PD-1 and CTLA-4 are both immunosuppressive molecules, but they have distinct roles within the immune response. CTLA-4 primarily operates in the early stages of T-cell activation by competing with CD28 for binding to CD80/86, resulting in the suppression of T-cell activation. In contrast, PD-1 inhibits the activity of T cells that are already activated, particularly those that have infiltrated peripheral tissues. According to a 2005 study by Contardi *et al.*, CTLA-4 was observed on the surface of 30 out of 34 neoplastic cell lines of various origin. Treatment of these tumors involved administering recombinant CD80 and CD86 ligands to induce apoptosis in these neoplastic cells presenting CTLA-4, and thus reducing Tregs activity in the tumor microenvironment [23]. However, CTLA-4 is expressed on Tregs elsewhere in the body, and monotherapy with the CD80/86 ligands, or anti-CTLA-4, may lead to generalized Tregs deficiency which can prompt inflammatory side effects elsewhere [24].

In many complicated cases, a tumor may become largely heterogenized, varying the TSAs that it expresses, or a partial-to-complete loss of expression altogether. Anti-CTLA-4 and anti-PD-1 monotherapies, categorized as ICB therapy, are effective in some tumors but face challenges in cases with inherent or acquired resistance [7]. Combining multiple agents is suggested to address tumor heterogeneity and prevent cancer recurrence, particularly in vaccine development [25, 26].

Within these pathways, several molecules and receptors stand out as ideal targets for stimulating immune cell activity in the tumor microenvironment. Due to the wide variety of factors that play a role in both suppressing and fostering neoplastic growth, an argument can be made to focus on any given number of cytokines, ligands, immune cells, antigens, etc., in order to ascertain which substance or substances are ideal targets for effective immuno-oncotherapy. The experiment was designed to evaluate the synergistic effects of specific substances

previously documented in multiple studies [27–30]. Namely, an antibody (Ab) known as anti-OX40, an oligodeoxynucleotide known as cytosine-phosphorothioate-guanine (CpG), and a ligand of retinoic acid-inducible gene I (RIG-1). The roles of these substances within the immune system and their effects on neoplastic cells are elaborated below.

1.1. OX40 and Anti-OX40

A key component to overcoming intratumoral immunosuppression is regulating the negative effects of Tregs within the microenvironment. Anti-OX40 is an agonistic antibody to OX40, a co-stimulatory molecule expressed on both T_{eff}s and T_{reg}s [24, 30]. OX40, which belongs to the TNFR superfamily, contains a cytoplasmic tail that can bind OX40 ligands present on many molecules in the immune signaling pathway (**Figure 1-3**), and induces expression of proteins that prolong T_{eff}s survival (eg. Survivin, B-cell lymphoma 2, B-cell lymphoma extra-large) [7, 31]. The addition of anti-OX40 enhances both CD4⁺ and CD8⁺ T-cell proliferation and their response to TSAs. Anti-OX40 therapy and ICB therapy differ in that anti-OX40 directly activates immune cells, rather than downregulating the occurrence of immune suppressors [7]. In one study, OX40 identified a group of high-affinity CD8⁺ T-cells that produced higher amounts of IFN γ in situ, and this number of CD8⁺ T-cells doubled when anti-OX40 and anti-CTLA-4 therapy were combined [32, 33]. Combinations of anti-OX40 and anti-CTLA-4 have also shown promising results in a 2014 study done in Oregon, noting that the combination of anti-CTLA-4 and anti-OX40 lead to noticeable tumor regression. Additionally, it induced the production of both Th1 cells, responsible for expressing IFN γ , and Th2 cells, which produce IL-4, IL-5, and IL-13. These latter three cytokines are linked to B-cell differentiation [14, 34].

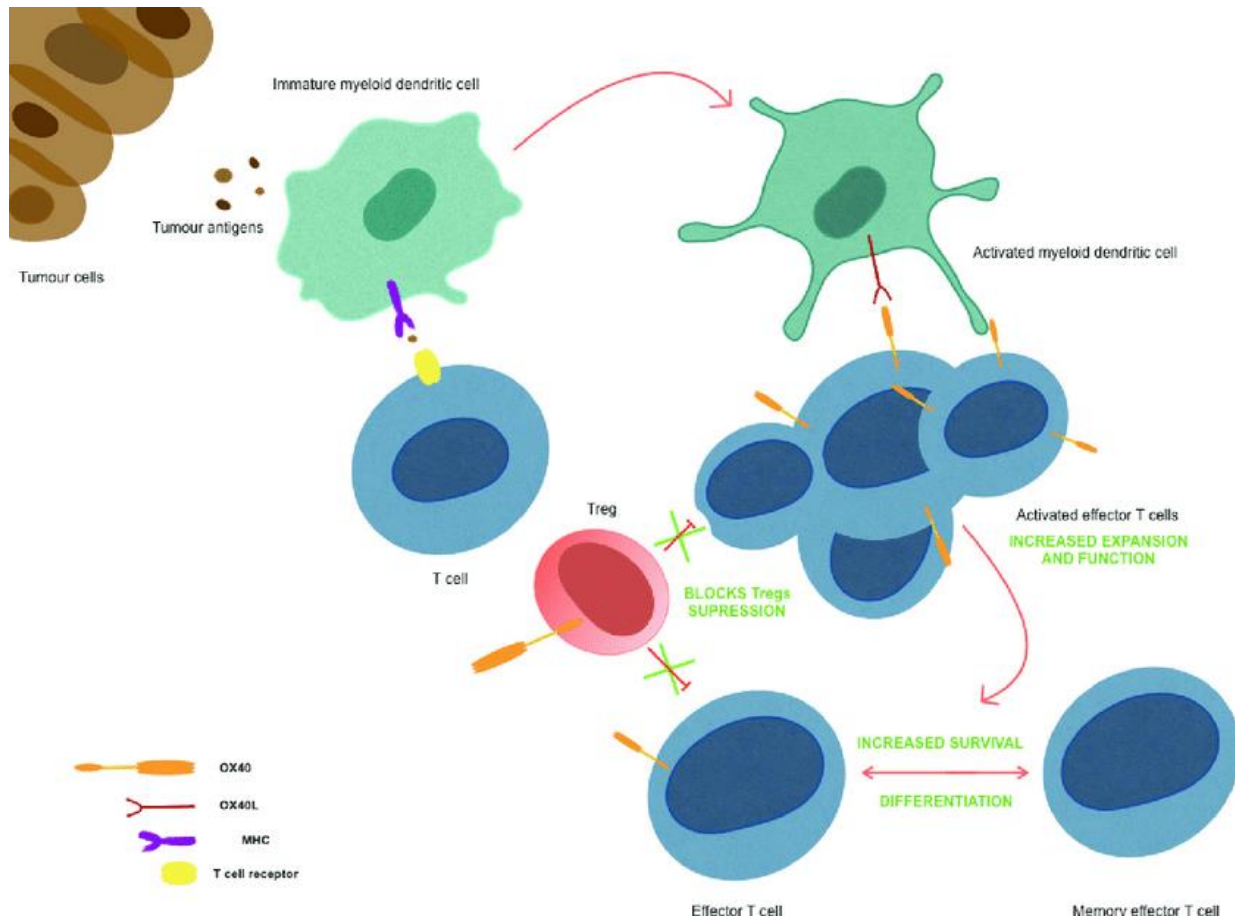


Figure 1-3: Basic mechanism of OX40 and OX40 Ligand (OX40L) as part of the T-cell activation pathway through major histocompatibility complexes (MHCs) present on myeloid dendritic cells. Anti-OX40 directly boosts expansion and function of effector T-cells, while simultaneously blocking the suppressive effects of regulatory T-cells (Tregs). This leads to a two-fold stimulation of effector T-cells [7].

Furthermore, a 2018 study from Zhang *et al.* shows that increased OX40 expression leads to an inhibition of FOXP3 expression, and consequently a downregulation of Tregs production. OX40 potentiates basic leucine zipper ATF-like transcription factor (BATF) and BATF3, whose activity can repress FOXP3 production in a closed chromatin configuration, suggesting that under the influence of OX40, the chromatin around the FOXP3 gene may become more tightly packed, making it less accessible for transcription factors and resulting in decreased FOXP3 expression [35]. In this way, OX40 essentially prevents naïve CD4⁺ T-cells from differentiating into Tregs, providing a way to reduce Tregs function without altering Teffs [36]. This response proves to be particularly advantageous in cancer patients, by rebalancing the tumor microenvironment and providing a way to overcome Tregs-mediated immune evasion. Due to

OX40 and anti-OX40 acting directly on T-cells, they can be applied to a wide variety of cancers without requiring in-depth insight on the specifics of a TSA's structure and can potentially overcome the issue of primary or acquired resistance found in ICB therapy [7, 26].

1.2. Cytosine-Phosphorothioate-Guanine

Cytosine-phosphorothioate-guanine, or CpG, is an oligodeoxynucleotide (ODN) ligand for Toll-like receptor 9 (TLR9). TLR9 is a transmembrane pattern recognition receptor (PRR) which commands a central role in recognizing pathogen-associated molecular patterns (PAMPs) expressed on a wide variety of infectious agents, and moderating a subsequent cytokine response to these agents via selective activation of nuclear factor κ B (NF- κ B) and other transcription factors [37, 38]. TLR9 encodes a deoxyribonucleic acid (DNA) binding site for CpG, which is commonly found in both bacteria and viruses [39, 40]. Once bound by CpG locally, TLR9 supports TSA presentation by prompting dendritic cell maturation. Mature dendritic cells will have improved antigen presentation of OX40L [27, 31]. TLR9 activation can also enhance natural killer (NK) cell function and stimulate proinflammatory cytokine production, among other effects [41].

CpG ODNs themselves have three unique categories based on structure and activity; CpG-A, CpG-B, and CpG-C. CpG-A ODNs induce plasmacytoid dendritic cells into producing high amounts of IFN α and TNF α , which promotes the activity of CD8⁺ cells and NK cells dependent on these cytokines. NK cells lack TLR9 and are thus dependent on the intermediary step provided by the APCs [42, 43]. However, they poorly signal NF- κ B, and induce a weak production of proinflammatory cytokines, such as IL-6. CpG-B, on the other hand, upregulates CD40, CD80, and CD86 expression, prompting APCs to promote maturation of more innate immune cells—particularly B-cells. This effect is likewise shown in a markedly increased expression of IL-6 and TNF α as opposed to CpG-A [43, 44].

CpG-C happens to express both characteristics of its predecessors, inducing cytokine expression of IFN α and TNF α , as well as production of IL-6. Type-C CpG is also capable of stimulating B-cells via the same route as CpG-B, leading to a far more complete and potent immunostimulatory effect as opposed to CpG types A and B [43, 44]. These characteristics render CpG-C an ideal substance for immunotherapeutic use in combination with anti-OX40.

1.3. CpG and Anti-OX40

Synergy between CpG and anti-OX40 has been extensively studied and documented in various research papers [27–30], noting that CpG-bound TLR9 potentiated OX40 expression on CD4⁺ T-cells, chiefly among T_{effs}. A 2018 Stanford study found that this effect was exclusive to OX40 and did not extend to the immune checkpoint inhibitors CTLA-4 and PD-1. Furthermore, the study revealed that in the absence of treatment, T-cells fail to maintain consistent OX40 expression after dendritic cells and macrophages are depleted *in vitro*, even with the addition of CpG. The conclusion they proposed is that CpG prompts myeloid cells to secrete cytokines, namely IL-12, IFN γ , and TNF α , which, in turn, promote the expression of OX40 on T-cells. This research highlights the significance of intermediary cytokine release in driving OX40 expression, both *in vitro* and *in vivo*. They also noted that the injection of CpG intratumorally upregulated the expression of OX40 locally, which initiated significant tumor regression, but had little to no effect in a distant and untreated tumor in the same host. Anti-OX40 alone had middling results as well, showing minor delays in tumor growth in both sites. However, with the combination of anti-OX40 and CpG, the pair were responsible for complete regression of both the treated and untreated A20 lymphomas [30]. CpG and anti-OX40 were able to maintain an efficient immune response without completely exhausting the necessary antibodies required for overcoming tumor expansion for long enough to see significant, if not total regression of the targeted tumors. Other studies have likewise noted the synergistic quality of administering both CpG and anti-OX40, and their therapeutic value in A20 B-cell lymphomas [28, 30, 45], hepatocellular carcinomas [27], Krebs-2 carcinomas, and Lewis lung carcinomas [45]. The latter two neoplasias were reported to have responded less effectively to CpG and anti-OX40 treatment than the formers, due to the weak immunogenicity of their TSAs [45]. Nevertheless, anti-OX40 and CpG remain promising agents for immunotherapy in various cancer types. Indeed, the combination of these immunostimulatory agents show encouraging results in treating even metastatic cancers [46]. We attempted to replicate these effects in an even more aggressive line of neoplastic cells, with the addition of a few more variables.

1.4. Retinoic Acid-Inducible Gene I

One of these new variables includes retinoic acid-inducible gene I, or RIG-I, a cytoplasmic ribonucleic acid (RNA) helicase that detects viral single- and double-stranded RNA. RIG-I is categorized as a member of the RIG-like helicases (RLH) group, which shares characteristics with another prominent class of PRRs, the Toll-like receptors. RIG-I, alongside melanoma differentiation-associated 5 (MDA5), and Laboratory of Genetics and Physiology 2 (LGP2) comprise the three pillars within the RLH family [38]. RLHs have been widely studied in connection to antiviral immune signaling, as they are able to bind to a variety of 5' uncapped triphosphate single- or double-stranded RNA from viral and host origin [47, 48]. RIG-I will typically bind to shorter ssRNA and ~1 kilo-base pair (kbp) dsRNA. In contrast, IFN production was found to be MDA5-dependent in ~2kbp dsRNA [48]. Both receptors contain a caspase active recruitment domain (CARD), which becomes exposed for signaling upon RNA binding. This binding leads to the recruitment of mitochondrial antiviral-signaling proteins (MAVS) on RIG-I. MAVS then initiates a signaling cascade involving various factors, such as tumor necrosis factor receptor-associated factor 3 (TRAF3), thirty-eight negative kinase 1 (TNK1), and inhibitor of NF- κ B kinase- ϵ (IKK ϵ) to activate interferon regulatory factors (IRF) 3 and 7 [49]. IRF3 and IRF7 are transcription factors which then enter the cell nucleus to induce type I and type III IFN production. The full pathway can be seen illustrated in **Figure 1-4** [50]. MDA5 activates a similar pathway to RIG-I, while LGP2, in contrast, does not possess a CARD and is instead believed to regulate other RLHs in the presence of IFNs [48].

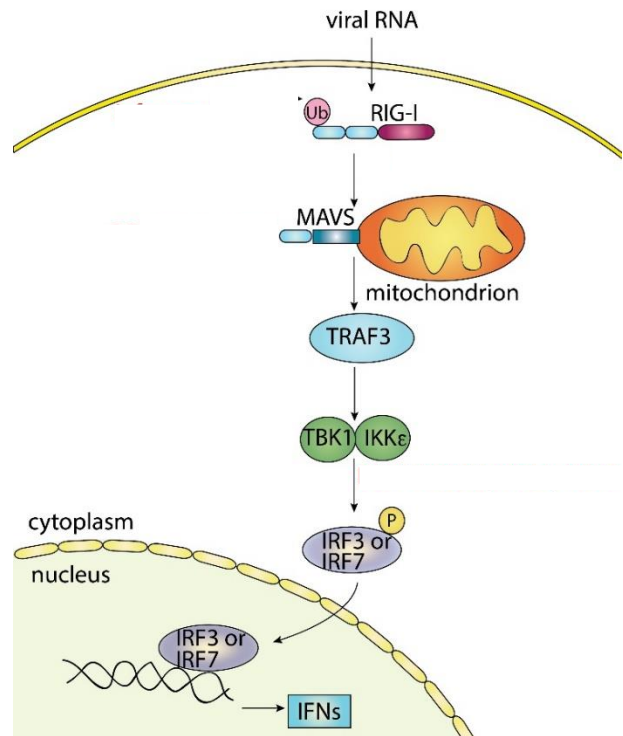


Figure 1-4: IFN induction pathway as signaled by RIG-I binding to viral RNA. RIG-I binding to RNA allows MAVS recruitment of factors TRAF3, TNK1, and IKK ϵ , leading to subsequent activation of IRF3 or IRF7. Finally, transcription factor binding to nuclear DNA allows IFN production. 'Ub' refers to a polyubiquitin chain, used to help viral RNA expose the RIG-I CARD, 'P' refers to phosphorylation of the Interferon Regulatory Factor (IRF) 3/7 [50].

In our case, we used a 5' triphosphate hairpin RNA (3p-hpRNA) synthetic influenza sequence to act as a RIG-I ligand to initiate transcription of type I IFNs. 5' triphosphate caps are not recognized by MDA5, ensuring this ligand will exclusively bind to RIG-I out of the three RLRs [51].

1.5. IL10, IL6, and IFN γ

In this section, we review the pathways through which IFNs and ILs are expressed and how they influence inflammatory processes. IFNs are categorized into types I, II, and III. Type I IFNs are produced by monocytes and fibroblasts, typically in response to a viral invasion. Viral DNA or RNA will bind to PRRs such as TLR9 or RIG-I, and through signal transduction pathways like the one provided in **Figure 1-4**, will incite IFN I production. Once produced, type-I IFNs will bind to their respective receptors, eventually leading to production of proteins that limit the replication of viral biopolymers [52]. Similarly, type III IFNs primarily elicit antiviral signaling pathways, and have been found especially potent in certain virus families— such as rotaviruses— in contrast to type I IFNs. Nevertheless, the two groups have closely linked signal transduction routes [53].

Type II interferons, however, consist entirely of IFN γ . IFN γ has a pleiotropic effect, including stimulating MHC I and II expression on APCs to enhance antigen presentation, activating innate immune cells, regulating the balance between Th1 and Th2, and mediating apoptotic pathways. IFN γ is produced by NK cells, CD8+ T-cells, and CD4+ Th1 cells, making it an ideal target for cytokine enzyme-linked immunosorbent assays (ELISA). Higher levels of IFN γ detected by the assay serve as an indicator of the activation of these innate immune cells. IFN γ expression is enhanced by cytokines like IL-12, IL-15, and IL-18, with IL-12 in particular forming a positive feedback loop with IFN γ . APCs can initially release IL-12 when activated by TLR9, prompting IFN γ production. This process is further amplified as macrophages, in the presence of IFN γ , release more IL-12, encouraging increased IFN γ secretion by activated T-cells and NK cells [54].

Cytokines in general rely on the Janus kinase (JAK)-signal transducer and activator of transcription (STAT)— or JAK-STAT— pathway. Cytokines lack individual kinase activity and rely on the JAK-STAT pathway for signal transduction and initiation of gene transcription within the cell nucleus. IFN γ and IL-12 are no different in this regard. Interleukins, such as IL-

IL-12, can interact with either type I receptors, often associated with proinflammatory responses, or type II receptors, which generally elicit anti-inflammatory effects. Once an interleukin binds to a cytokine receptor, they initiate the JAK-STAT pathway. IL-12 will bind to a type I receptor, which leads to an activation of JAK2 and subsequently STAT4, and this polymer prompts target gene expression of IFN γ [55]. Once IFN γ becomes active in the host, it will undergo its own JAK-STAT signal transduction, recruiting JAK1 and JAK2 to the IFN γ and IFN γ -receptor dimer. JAK1 and JAK2 are phosphorylated and will, in turn, phosphorylate STAT1, which couples and induces transcription of interferon-stimulated genes (ISG). These ISGs code for numerous IFN-dependent proteins, which then go on to mediate the effects described above, notably activating innate immune cells via MHC regulation, activating NK cells, and promoting Th1 cell development and differentiation [56]. An illustration of this feedback loop, including the JAK-STAT interactions of IL-12, can be seen in **Figure 1-5** [57].

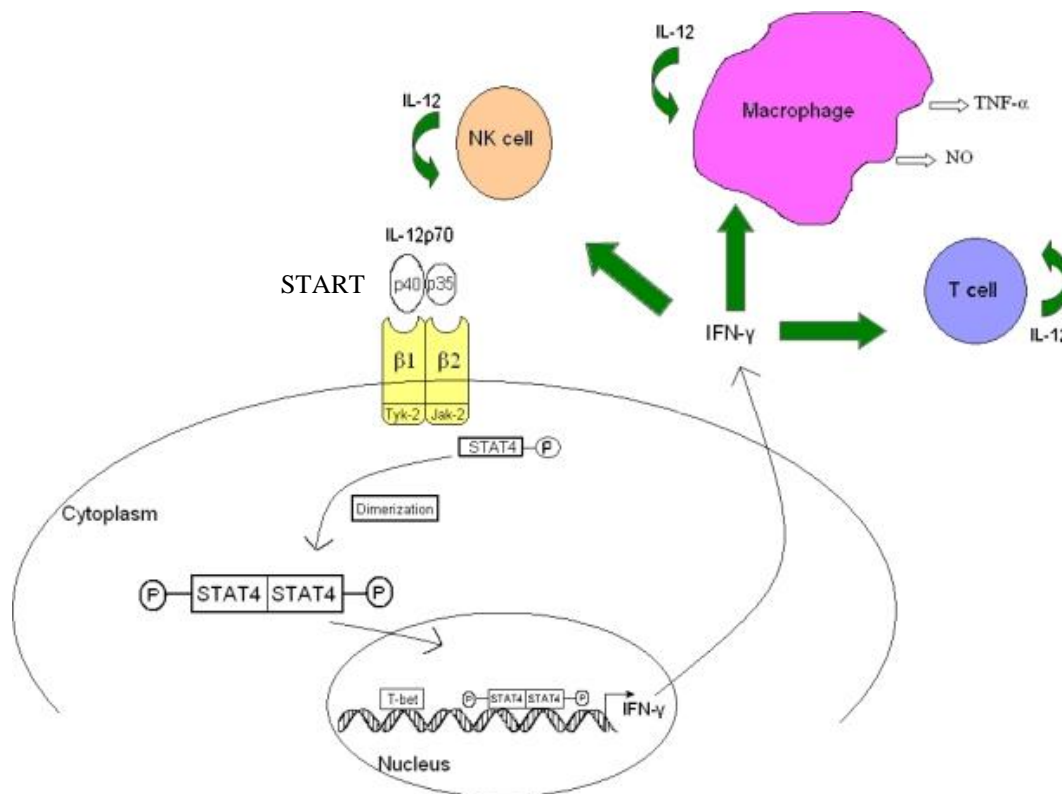


Figure 1-5: Positive feedback loop of IL-12 and IFN γ . The loop begins with IL-12 bound to p40 and p35 subunits. JAK-2, along with tyrosine kinase-2 (Tyk2) will recruit phosphorylated STAT4. The dimer moves into the nucleus to induce IFN γ production. IFN γ in turn activates NK cells, T-cells, and macrophages (represented in straight green arrows). IFN γ induces macrophages in particular to release more IL-12, and the cycle starts anew [57].

IL-6 likewise has a pleiotropic immunostimulatory effect, so much so that it was previously thought to be at least four separate molecules. These four were B-cell stimulatory factor 2 (BSF-2), hybridoma growth factor (HGF), IFN- β 2, and hepatocyte-stimulating factor (HSF). These factors were found to be identical in 1989, earning them the common name of IL-6. IL-6, as the previous names suggest, has a direct effect on B-cell maturation into Ab-producing cells, B-cell stimulation to fuse with myeloma cells, IFN-like antiviral abilities, and stimulating protein synthesis in liver cells, respectively [58, 59]. With these effects in mind, the pathway through which IL-6 exercises an inflammatory response becomes clearer. In the context of immunotherapy, IL-6 is primarily characterized as a proinflammatory cytokine, with inhibitory effects on Tregs via inhibiting FOXP3 expression. Once IL-6 is synthesized by T-cells or monocytes at the site of inflammation, the cytokine travels through the bloodstream to the liver, where hepatocytes are one of the few cell types presenting IL-6 receptor (IL-6R). Once bound to IL-6R, a type I cytokine receptor, the complex will initiate cellular signaling through the JAK-STAT pathway– in this case JAK1, STAT1, and STAT3. Once dimerized, the complex enters the nucleus to promote IL-6 target genes, including those coding for other proinflammatory cytokines, leading to further activation of the immune response [60].

IL-10, as previously mentioned, exerts its immunosuppressive effect by downregulating Th1 cytokines, MHC antigens, and macrophage costimulatory molecules. The action of IL-10 is essential to host survival, as the unchecked action of proinflammatory molecules in response to an infection can lead to dangerous side effects. Excess presence of IL-10, however, will completely suppress the inflammatory cells, resulting in a lack of disease clearance. The interactions between IL12, IL10, and IFN γ are illustrated in **Figure 1-6** [19].

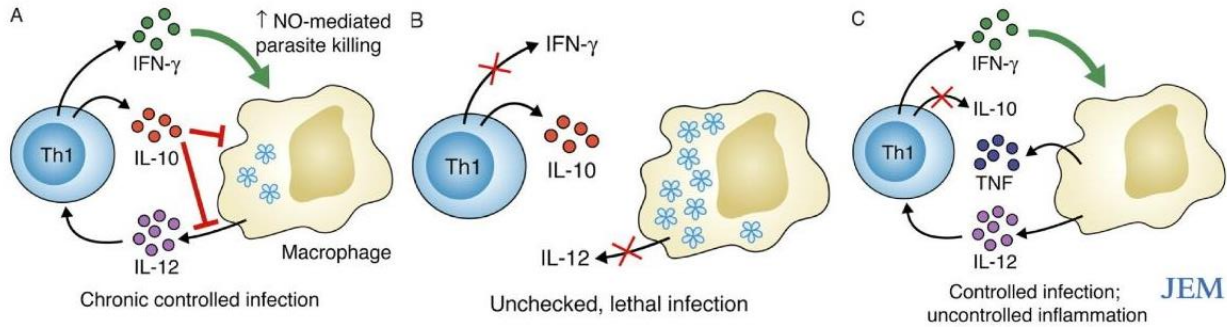


Figure 1-6: Three types of interactions between T-helper 1 (Th1) release of Interleukin-10 (IL-10), Interleukin-12 (IL-12), and Interferon γ (IFN γ) in the presence of a parasitic infection. (A) IL-10, IFN γ , and IL-12 are all produced in equal amounts. IL-10 prevents overproduction of IFN γ and IL-12, meaning the three cannot effectively eradicate intracellular parasites (represented by blue flowers). (B) IL-10 and parasites block both IFN γ and IL-12, leading to no inflammatory response and an overpopulation of parasites. (C) IL-10 production is entirely stopped, leading to overproduction of IFN γ and IL-12. This eliminates the parasites but can damage surrounding tissue [19].

As depicted in **Figure 1-6** above, the balance between IL-10-mediated immunosuppression and IFN γ /IL-12-mediated immunomodulation is intricate. As mentioned earlier, most tumors can overproduce IL-10 within their microenvironment, disrupting this balance and favoring immunosuppression. This facilitates unchecked tumor cell proliferation, highlighting the importance of measuring IL-10 levels in ELISA tests for evaluating the efficacy of immunostimulatory molecules on both untreated and treated tumors.

1.6 The RENCA CRL-2947 Cell Line

Naturally, the efficacy of these low molecular weight substances (CpG, anti-OX40, and RIG-I ligand 3p-hpRNA) also depends on the neoplastic cell line. Renal carcinomas, or RENCA, account for the majority of kidney diseases, with the RENCA cell line we used being reported as particularly invasive and highly proliferative. While it is not a typically metastatic cell line, it has been known to cause some secondary neoplasias, especially in the lung and liver. As mentioned earlier, while CpG and anti-OX40 have demonstrated statistically significant results in many A20 lymphoma experiments, the synergistic effects were less pronounced in Krebs-2 carcinomas and Lewis-lung carcinomas due to their poor immunogenicity [45]. In this context, we inoculated and observed a renal carcinoma first isolated from BALB/c mice, known as RENCA CRL-2947, as it has not yet been characterized in this context.

The aim of using this cell line is to attempt to find a combination of immunostimulatory agents which efficiently reduces growth of this adenocarcinoma, as kidney neoplasias have a

particularly poor prognosis among the cancer varieties present *in vivo* [61]. This is because early tumor stages often lack clinical symptoms, and by the time the cancer is diagnosed, it may be too advanced for effective treatment [62]. In a previous experiment done by the department of Microbiology and Infectious Diseases at the University of Veterinary Medicine in Budapest, this cell line was used in combination with similar low molecular weight substances but did not achieve significant reduction of tumor size, nor any marked increase in median survival time. Based on this study, treatment was administered at an earlier date, prior to the substantial formation of a primary tumor site, as well as the addition of more treatment groups to accurately monitor the effect of each substance on tumor growth [63].

2. Aims

This study intended to investigate the antitumor properties of three immunotherapeutic agents in 40 mice injected with the RENCA CRL-2947 cell line. Our objective was to observe and quantify these effects within three distinct treatment groups: (1) CpG ODN with anti-OX40, (2) CpG ODN with a RIG-I ligand, and (3) the same RIG-I ligand as monotherapy. Each treatment was administered to ten mice, with the final ten control mice receiving phosphate-buffered saline (PBS) in lieu of treatment. Antitumor properties were observed and quantified by measuring average tumor size, median survival time, proinflammatory cytokine production, and reduction of metastasis.

3. Materials and Methods

3.1. Cancer Cell Line

As previously stated, we utilized a RENCA CRL-2947 kidney-derived mouse adenocarcinoma cell line purchased from ATCC (Manassas, Virginia, USA). The cells were grown on Roswell Park Memorial Institute (RPMI) 1640 medium (Merck, USA) composed of 10% fetal calf whey, non-essential amino acids, L-glutamic acid, and sodium pyruvate. The cell culture was incubated at 5% CO₂ and 95% humidity at 37°C until a desired pH of 7.0-7.6 was achieved. Once the cell layer had become established, the culture was rinsed with 0.25% trypsin-0.53 mM ethylenediaminetetraacetic acid (Merck, USA) solution to remove the medium containing the trypsin inhibitor. Once the cells had settled, they were suspended for fetal calf whey-free RPMI. The viability of the final cell culture was checked with a 0.4% Trypan blue (Thermo Fischer Scientific, USA) staining to identify any dead cells.

We used 40 adult pathogen-free BALB/c female mice weighing 45-50 grams (Charles River, Germany). The mice were kept in groups of ten inside the animal laboratory of the National Food Chain Safety Office Directorate of Veterinary Diagnostics. The room was kept at a temperature of $20 \pm 2^\circ\text{C}$ and a humidity of $50 \pm 10\%$, with *ad libitum* food and water. The mice were checked at least once a day to ensure these conditions were consistently met, and that the animal welfare directives set by the National Food Chain Safety Office, the Committee of Animal Welfare at Work, and the Government Office of Pest County were likewise met throughout the duration of the experiment.

It is important to note that although all mice were kept in groups and monitored regularly, BALB/c mice are prone to exhibiting cannibalistic behavior, ranking as the second most frequent mouse line to do so [64]. While we made efforts to minimize stress, we were unable to completely eliminate this behavior. Cannibalism only occurred after mice had succumbed to tumor-related disease, but this meant that there were fewer samples to examine histologically in later phases of the experiment.

In total, the 40 mice were each implanted with 200 μ l of the RENCA CRL-2947 cell suspension at a concentration of 3×10^5 /ml. The cells were injected subcutaneously into a fold of skin above the *musculus biceps femoris*. During administration, the mice were properly fixed, and the injected needle was aspirated to ensure correct subcutaneous implantation prior to injection. Once injected and the needle was removed, pressure was applied to the area for 5-7 seconds to ensure the cells remained in the subcutis. The mice were then randomly assigned to four groups of ten to establish sample groups.

3.2. Dosages and Course of Treatment

The three primary reagents used for treatment were selected based on previous experiments done by the Department of Microbiology and Infectious Diseases, and each substance was purchased by the department from varying suppliers. The unmethylated CpG oligodeoxynucleotide (Class C CpG oligonucleotide – Multispecies TLR9 ligand) was purchased from Invivogen (San Diego, California, USA) in 200 μ g lyophilized cases.

The rat monoclonal anti-CD134 / OX40L receptor antibody (anti-OX40) was purchased from Abcam (Cambridge, UK). The first group of 10 mice each received 50 μ g of CpG and 5 μ g of anti-OX40 dissolved together in 200 μ l of pyrogen-free water (Merck Millipore, USA). These substances were injected together intratumorally on all 3 treatment dates.

The second group likewise each received 50 μ g of CpG, but this was simultaneously administered with 3 μ g of a 5' triphosphate hairpin RNA (3p-hpRNA) RIG-I, which was likewise purchased from Invivogen (San Diego, California, USA). This 3p-hpRNA RIG-I ligand is a synthetic negative single stranded RNA which has been adapted from H1N1 influenza A virus. The unique structure of this ligand ensures that it will exclusively bind to RIG-I and no other PRRs. These two substances were similarly dissolved in 200 μ l of pyrogen-free water and administered to each mouse in group two. Mice in group three received 3 μ g of this 3p-hpRNA

suspended in 200µl of pyrogen-free water exclusively. In contrast, the untreated group received injections of 200µl phosphate-buffered saline (PBS) on the same days, in order to reduce variability in the results.

The initial treatment was administered on day 10 following implantation when tumor sizes ranged from 2 to 7 cubic millimeters, or just barely palpable. The aforementioned dosages were injected intratumorally to each mice, corresponding to their treatment group. Subsequent treatments were given on day 14 and day 17, wherein all three treatment groups received the same combination and dosage. The control group remained untreated. Measurements of primary tumor sizes were conducted using a standard caliper following the final treatment on day 17 and subsequently every seven days until day 38.

3.3. Cell Pre-Experiment

The dosages of all three treatment groups were determined based on previous experiments by the Department of Microbiology and Infectious Diseases, and an *in vitro* pre-experiment conducted in the department lab. The pre-experiment was conducted 4 months prior to the *in vivo* experiment and examined the viability of swine peripheral blood mononuclear cells when exposed to varying dosages of the aforementioned substances. Four groups were formed, with group one examining the cytotoxic effect of 100µg CpG + 10µg anti-OX40, 50µg CpG + 5µg anti-OX40, and 25µg CpG + 2.5µg anti-OX40. Group two had the same three dosages of CpG, but in lieu of anti-OX40 received 6µg, 3µg, and 1.5µg of 3p-hpRNA RIG-I ligand instead. Group three received the same three doses of 3p-hpRNA alone, and group four received 1000ng, 500ng, and 250ng of a lipopolysaccharide as a control. The middle dosage in each experiment group was the highest concentration of treatment substances to show no cytotoxic effect while being cost-effective, and as such were chosen as the dosages for the *in vivo* experiment.

3.4. Measurement of Cytokine Production

Concurrently to the primary experiment, we conducted an additional study involving eight BALB/c mice to assess total target cytokine production as induced by the treatment substances or tumor cells. Among these mice, two received no treatment and were implanted with 200µl of RENCA CRL-2947. The remaining six mice were not implanted with tumors but were instead assigned to three treatment groups: CpG + anti-OX40, CpG + 3p-hpRNA, and 3p-hpRNA alone,

with two mice in each group. Each mouse received the same treatment dosages corresponding to those used in the primary experiment for their respective groups. On day 7 of the experiment, we euthanized and collected blood samples from the two tumor-implanted mice, and on day 32 we euthanized the remaining six mice. Once all eight samples were collected, we conducted standard cytokine ELISA tests to measure IFN- γ , IL-6, and IL-10 production in each group.

3.5. Postmortem Data Collection

During the course of the *in vivo* experiment, all of the mice were checked daily, and any dead mice were promptly dissected using stainless steel autopsy scissors and anatomical forceps. Following a brief external examination, the mice were opened with an abdominal incision, where the primary tumor size and any visible anomalies were noted, as well as positioning of internal organs and presence of ascites. The aim of the postmortem examinations was primarily to note any obvious signs of metastasis and secondary disease. Spontaneously arising renal adenocarcinomas typically metastasize in the lungs and liver, and as such the spleen, liver, kidneys, and lungs were removed and stored in an 8% formalin mixture to suspend the organs until the microscopic examination at the end of the experiment. The entire primary tumor was excised in all patients when possible, and consistency, size, and shape were noted, as well as any clear demarcation, necrosis, or inflammation if present. In cases where the entire removal of the primary tumor was impossible, a large sample section was excised along the border between the affected and unaffected tissue instead. These samples were similarly suspended in 8% formalin.

The organ and tumor samples were placed into labeled containers, noting the treatment group and dissection date of each mouse. The samples were then processed in the laboratory of the Directorate of Veterinary Diagnostics within the National Food Chain Safety Office. Cross sections of each organ were cut, labeled, and prepared with a standard hematoxylin-eosin staining procedure. Once the samples were dry, a microscopic examination was conducted. During the microscopic exam, signs of metastasis or secondary disease in each organ were noted when present, as well as the histological appearance of the primary tumor.

3.6. Post-Experiment

The experiment was terminated on day 39 post-implantation due to noticeable declines in animal health and well-being. Factors such as mobility, stress levels, and overall quality of life had significantly deteriorated, and so we conducted humane euthanization of the animals through CO₂ anoxia. No anesthesia or analgesics were administered, as the stress induced by their administration is thought to potentially exceed the discomfort associated with euthanasia. The euthanasia procedure adhered to swift and humane protocols in accordance with the guidelines set by the National Institute of Health in the "Guide for the Care and Use of Laboratory Animals". By this time, all relevant data had been collected, and the euthanized mice were dissected in the same fashion as described above.

3.7 Data Analysis

We visualized the average survival time for each group through a Kaplan-Meier survival analysis graph and assessed the data points for statistical significance using the Mantel-Cox (log-rank) test, with a significance level set at $p < 0.05$. Furthermore, we conducted a Mann-Whitney test to determine the statistical significance of the average tumor sizes, comparing each treatment group's data to that of the PBS control group.

4. Results

4.1. Assessment of Median Survival Times

Any deaths observed during daily checks were documented on the corresponding day's chart. The initial death took place on day 21, involving two mice in the untreated PBS group. We continued to note every death until the termination of the experiment on day 39. The charted data are shown in the Kaplan-Meier survival analysis graph below (**Figure 4-1**). On day 38, the remaining mice in each treatment group were compared to the surviving mice in the control group using a Log-rank Mantel-Cox statistical analysis test ($p < 0.05$ threshold). The untreated PBS control group had a survival rate of 20%. Group one (CpG + antiOX40) had a survival rate of 70%, which led to a p-value of 0.0103 when compared to the untreated group. Group two (CpG + RIG-I Ligand) had a survival rate of 50%, which resulted in a p-value of 0.2465 in comparison to the control, while group three (RIG-I – 3p-hpRNA) had a survival rate of 60%, leading to a p-value of 0.0467. Groups one and three exhibited statistically higher survival times, while group two did not demonstrate significant differences compared to the survival times of the control group. All statistical results regarding medial survival time can be seen in **Table 4-1**.

Survival of CpG + anti-OX40, CpG + 3p-hpRNA, 3p-hpRNA, Untreated (PBS)

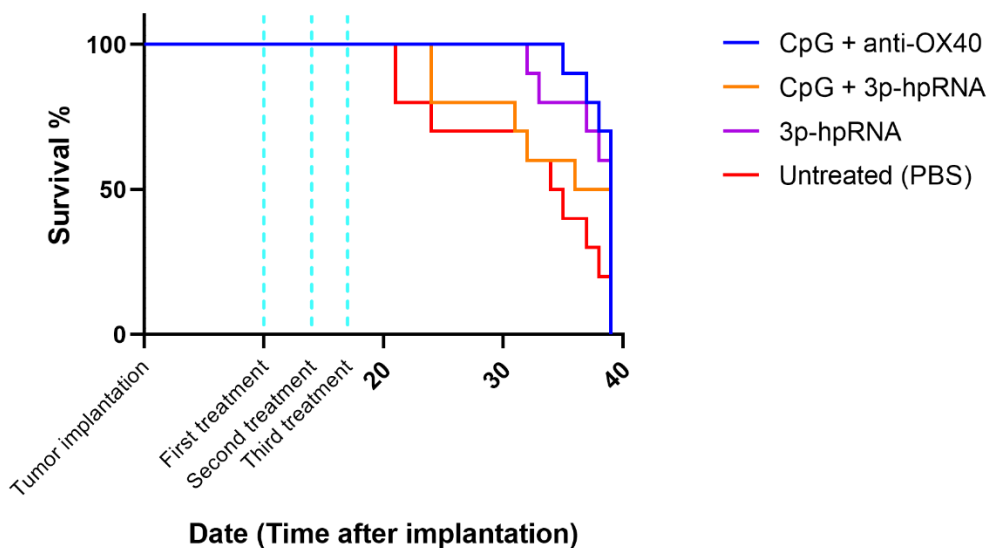


Figure 4-1: Survival times of total 40 mice over the course of 40 days. Percentage of living mice is represented as a function of surviving mice (%) over days since tumor implantation. Group one (CpG and antiOX40) is shown in blue, group two (CpG and RIG-I Ligand - 3p-hpRNA) shown in orange, group three (RIG-I Ligand - 3p-hp-RNA) shown in purple, and the untreated PBS control group shown in red. Treatments are represented by cyan dashed lines, and were administered on days 10, 14, and 17.

Table 4-1: Statistical results of treated groups in comparison to the untreated control. Analysis conducted using Mantel-Cox log-rank tests. Groups are colored in accordance with the lines presented in **Figure 4-1**. (Survival curves comparison)

1. **CpG + anti-OX40** vs. **Untreated (PBS)** → significant (p=0,0103)
2. **CpG + 3p-hpRNA** vs. **Untreated (PBS)** → not significant (p=0,2465)
3. **3p-hpRNA** vs **Untreated (PBS)** → significant (p=0,0467)

4.2. Primary Tumor Growth

In addition to median survival time, we also examined the rate of primary tumor growth as another variable. We conducted measurements of tumor size in all four groups on days 17, 24, 31, and 38 post-implantation to assess the differences between the treated and control tumors. The results are shown in **Figure 4-2** as a function of size over time. Each data point represents the average tumor size in the remaining mice in each group.

Statistical analysis of these values was conducted using a Mann-Whitney test (p<0.05 threshold), comparing each treatment group to the untreated PBS control on each day of measurement. Day 17 showed no significant disparities in primary tumor sizes between the different groups. Group one (CpG + anti-OX40) resulted in a p-value of 0.1232. Group two (CpG + RIG-I ligand 3p-hpRNA) and group three (RIG-I ligand 3p-hpRNA) likewise lacked statistical significance, with p-values of 0.9020 and 0.0572 respectively. Day 24 was the first to show any significant differences in tumor sizes, in both groups one (p=0.0001) and two (p<0.0001). Group three, however, generated a p-value of 0.1591. Day 31 continued along this same vein, with Groups one and two yielding p-values of 0.0007 and 0.0006 respectively. Group three continued to show non-significant differences in tumor size compared to the control, with a p-value of 0.8889. By day 38 the sample sizes of each group were too low to produce significant results. Analyses of groups one (p=0.0556), two (p=0.1786) and three (p=0.6667) resulted in no significant differences in tumor sizes between any of the treatment groups when compared to the control. All statistical results regarding primary tumor growth can be seen in **Table 4-2**.

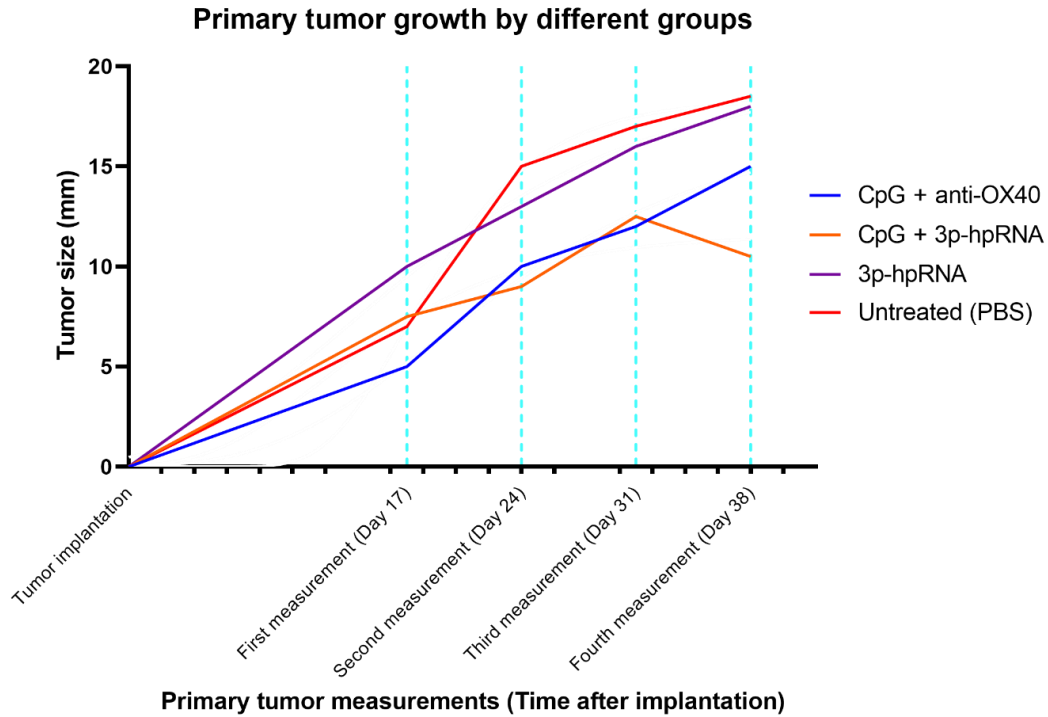


Figure 4-2: Primary tumor growth Figure 4-2: Primary tumor growth as shown as a function of size over time. Group one (CpG and antiOX40), shown in blue, group two (CpG and RIG-I Ligand - 3p-hpRNA) shown in orange, group three (RIG-I Ligand - 3p-hp-RNA) shown in purple, and the untreated PBS control group shown in red. Days where all tumors were measured are shown in dotted cyan lines, and were taken on days 17, 24, 31, and 38.

Table 4-2: Statistics: Mann-Whitney test (Treated Groups Compared to Untreated PBS Group)	
ns. – Not significant. sign. – Significant. Groups are colored in accordance with lines in Figure 4-2 .	
Day 17:	CpG + anti-OX40 (ns. - 0,1232), CpG + 3p-hpRNA (ns. - 0,9020), 3p-hpRNA (ns. - 0,0572)
Day 24:	CpG + anti-OX40 (sign - 0,0001), CpG + 3p-hpRNA (sign. <0,0001), 3p-hpRNA (ns. 0,1591)
Day 31:	CpG + anti-OX40 (sign. - 0,0007), CpG + 3p-hpRNA (sign. - 0,0006), 3p-hpRNA (ns. - 0,8889)
Day 38:	CpG + anti-OX40 (ns. - 0,0556), CpG + 3p-hpRNA (ns. - 0,1786), 3p-hpRNA (ns. - 0,6667)

4.3. Cytokine ELISA Tests

The eight mice involved in the preliminary cytokine production test were sampled and tested for IFN- γ , IL-6, and IL-10 production using a standard cytokine ELISA. The results of this preliminary study are presented in **Table 4-3** below. Total cytokine production was measured in picograms per milliliter.

Table 4-3: Eight mice tested for total production of three cytokines (IFN-γ, IL-6, IL-10). Mice implanted with 200 microliters of RENCA CRL-2947 are noted in the table as “Tumor +”. Those that were not implanted are marked as “Tumor –”			
Cytokine ELISA Results Preliminary Test	IFN-γ (pg/ml)	IL-6 (pg/ml)	IL-10 (pg/ml)
Tumor +, no treatment I.	neg.	neg.	350
Tumor +, no treatment II.	13,125	neg.	190
Tumor –, CpG + anti-OX40 I.	neg.	neg.	neg.
Tumor –, CpG + anti-OX40 II.	72,5	neg.	neg.
Tumor –, CpG + 3p-hpRNA I.	13	34	neg.
Tumor –, CpG + 3p-hpRNA II.	6,5	neg.	neg.
Tumor –, 3p-hpRNA I.	12,5	neg.	neg.
Tumor –, 3p-hpRNA II.	37,5	neg.	neg.

Nearly all treated groups exhibited varying levels of IFN- γ , with the exception of Tumor +, no treatment I and Tumor –, CpG + anti-OX40 I. Each column of the examined cytokines is visualized in separate graphs, shown in **Figures 4-3, 4-4, and 4-5**. The results of the IFN- γ production are represented in **Figure 4-3**.

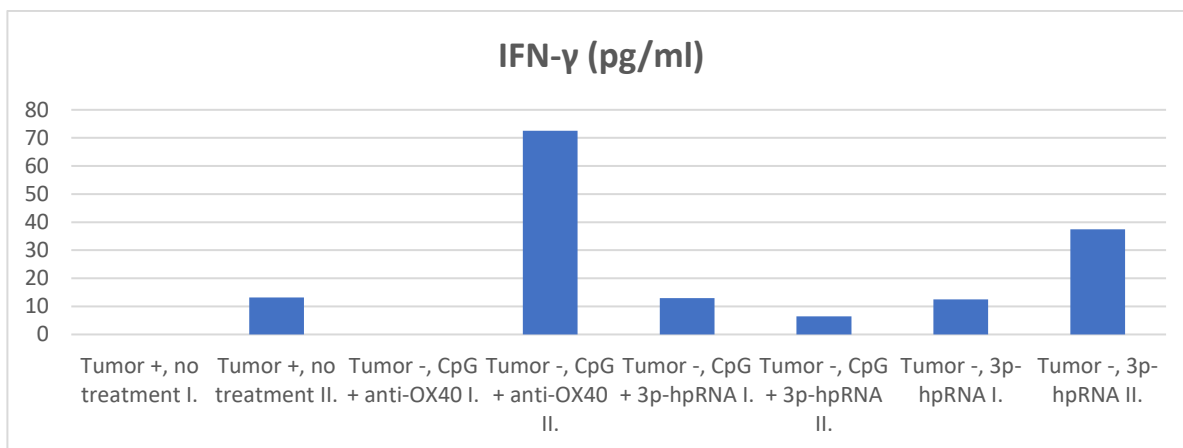


Figure 4-3: Total Interferon- γ (IFN- γ) production in eight mice. Treatment and tumor presence is noted under each bar along the x-axis. IFN- γ production is presented in picograms per milliliter.

The results of IL-6 production are represented in **Figure 4-4** below. Only one mouse presented any level of IL-6 production (Tumor –, CpG + 3p-hpRNA I).

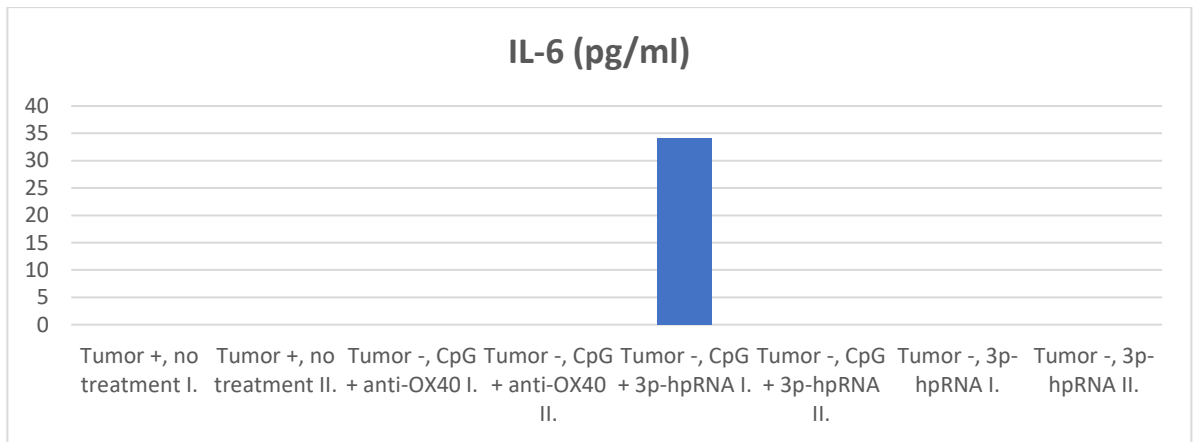


Figure 4-4: Total interleukin-6 (IL-6) production in eight mice. Treatment and tumor presence is noted under each bar along the x-axis. IL-6 production is presented in picograms per milliliter.

The data presented in the IL-10 column in **Table 4-3** are visualized in **Figure 4-5** below. The only two mice to result in any significant IL-10 production were the two mice implanted with RENCA CRL-2947.

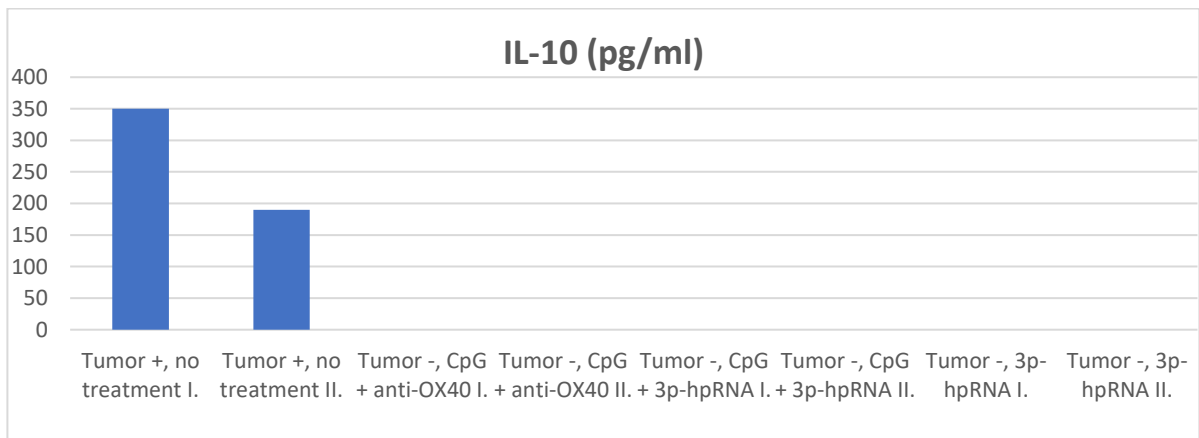


Figure 4-5: Production of interleukin-10 (IL-10) in eight mice. Treatment and tumor presence is noted under each bar along the x-axis. IL-10 production is presented in picograms per milliliter.

4.4. Reduction of Metastases

The final variable examined was to record the total incidence of metastasis in each group, including the untreated (PBS) control. Organs affected by metastasis in each group are listed in **Table 4-4** below. As mentioned earlier, the total number of mice in each group is less than 10, as we lost organ samples due to occasional cannibalistic behavior.

In some instances, we were unable to identify specific metastases, as the primary tumor seemed to disseminate within the abdominal cavity. While these events may not fit the traditional definition of metastasis, they still represented an uncontrolled spread of tumor cells,

so we included these cases in the final count of the “Abdominal Cavity” column in **Table 4-4**. This has been noted with an asterisk (*).

Table 4-4: Metastatic occurrence in each of the tested groups. Locations of metastasis are noted in each column, with the total number of metastatic events in each group listed in the far-right column.
** Disseminated tumor cells found in the body cavity, counted in the total number of metastatic events despite not falling under the definition of traditional metastasis.*

Treatments	Mice with metastases (%)			
	Lung	Kidney	Abdominal cavity*	Total
CpG + anti-OX40	29 (2/8)	0	0	29 (2/8)
CpG + 3p-hpRNA	11 (1/9)	0	22 (2/9)	33 (3/9)
3p-hpRNA	38 (3/8)	0	0	38 (3/8)
Untreated (PBS)	44 (4/9)	0	33 (3/9)	78 (7/9)

Treated groups one, two, and three showed metastasis in 29%, 33%, and 38% of cases, respectively. In contrast, the untreated (PBS) group saw metastasis in 78% of mice. Notably, we found two cases of metastasis that did not fall into any of the categories listed in **Table 4-4**. The first was an ovarian and the other was determined to be pancreatic metastasis. Upon histological examination of the tumor samples, we found visible differences in primary tumor characteristics. The treated groups (CpG + anti-OX40, CpG + 3p-hpRNA, and 3p-hpRNA) displayed early signs of demarcation. Meanwhile, the untreated group exhibited diffuse primary tumors accompanied by necrosis. Histological examples of lung metastasis (**Figure 4-6**) and a representation of the primary tumors' general appearance (**Figure 4-7B**) are provided below. Included in these images is a macroscopic view of how these tumors typically appeared in the mice (**Figure 4-7A**).

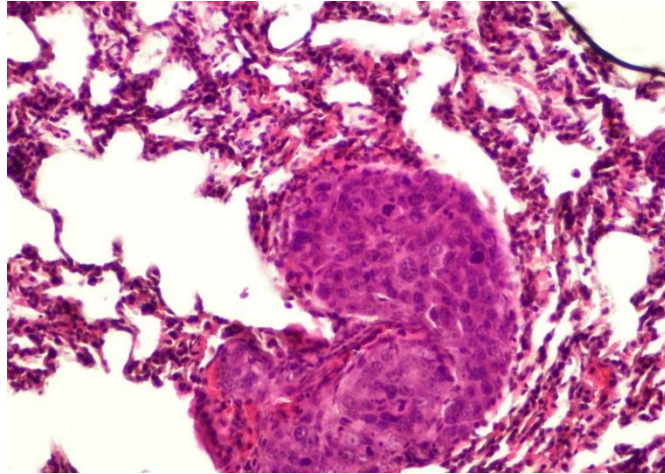


Figure 4-6: Histological slide of a lung metastasis from RENCA CRL-2497 tumor cells stained with haematoxylin-eosin. Abnormal aggregation of cells can be seen in the lower center of the image, lacking the typical appearance of lung tissue.

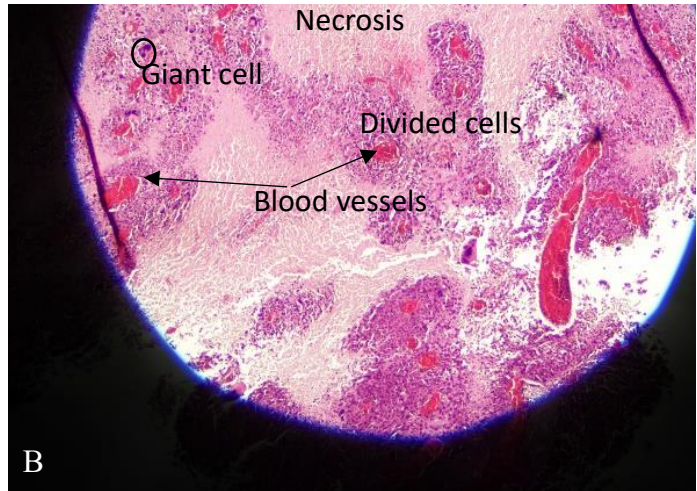


Figure 4-7: Macroscopic (A) and histological (B) appearance of a typical RENCA CRL-2947 primary tumor. Image 4-7A depicts the primary tumor, well encapsulated in the abdominal cavity of a BALB/c mouse. Abdominal organs have been removed. Image 4-7B notes the presence of Giant cells, Necrosis, Blood vessels, and Divided cells.

5. Discussion

After concluding the experiment, we deem the treatments to hold considerable promise. Notably, while the treatment effects were sustained, tangible outcomes were achieved: prolonged survival of the mice, reduction in primary tumor sizes, and mitigated metastatic formation.

With the first treatment group (CpG and anti-OX40), we expected to see an increased median survival time in comparison to the treatment group, based on previous experiments with similar variables [27–30, 45, 46]. With regards to the second treatment group, we investigated the combined effects of CpG with RIG-I ligand 3p-hpRNA to ascertain whether a similar stimulatory effect could be achieved with the substitution of anti-OX40. RIG-I ligand 3p-hpRNA was examined independently in the third control group to obtain more precise data regarding its stimulatory effects, given that it has not been as extensively described compared to the previous two substances. To put this succinctly, we aimed to investigate whether this 3p-hpRNA could activate the same immune pathways as CpG, considering that the receptors for both substances arise from different branches within the same family of PRRs. Ideally, the median survival times of all three groups would be, on average, higher than that of the control group. While this was true for groups 1 and 2 on days 24 and 31, the significant differences did not last until the final measurement.

As stated previously and shown in **Figure 4-1**, the survival rates on day 38 for groups 1, 2, and 3 were 70%, 50%, and 60%, respectively. The control had 2 out of 10 mice remaining by day 38, meaning the n-value of the data was not large enough to accurately elicit any significant differences when accounting for standard deviation. The large decrease in tumor size seen on **Figure 4-2** (Group 2, **Orange**: CpG + RIG-I ligand 3p-hpRNA, Day 38) is likely due to the decreased number of mice alive at this time. Only 50% of mice remained in group 2 by day 38, thus it is plausible that the mice in this group with relatively larger tumors had already perished/had been euthanized. This leads to a somewhat drastic decrease in tumor size, indicating a potential for survivorship bias. The fact that we observed statistical significance in tumor sizes in the middle of the experiment could suggest that the treatment substances were at

least somewhat effective at reducing the tumor growth rate, but due to the small sample size on day 38 we cannot confirm this as fact.

Regarding cytokine production, as mentioned earlier, tumors naturally produce anti-inflammatory cytokines such as IL-10. Our treatment substances were expected to shift this balance by deactivating anti-inflammatory processes and inducing production of proinflammatory cytokines such as IL-6 and IFN- γ . We anticipated that two untreated mice with implanted tumors would produce higher levels of IL-10, whereas the six tumor-less treated mice were expected to exhibit elevated levels of IL-6 and IFN- γ . Since the treated mice did not have implanted tumors, we measured only baseline cytokine production, without interference from neoplastic cells. If proinflammatory cytokines are detected in these otherwise healthy mice, it may suggest that the targeted immunostimulatory pathways have indeed been activated.

Overall, there are some visible trends in the data as seen in **Table 4-3**. The tumor positive, untreated mouse I did not produce either IFN- γ or IL-6, whereas tumor positive untreated mouse II showed some level of IFN- γ production. When we consider the IL-10 production in untreated mouse II, which was lower than in the other untreated mouse, it suggests that the tumor microenvironment may not have reached complete immunosuppressive levels. However, the exact reasons for these results remain unclear.

With regards to IFN- γ in the treated mice, besides no detection in one CpG + anti-OX40 mouse, all other treated mice exhibited IFN- γ production, suggesting successful immune activation in these cases. The absence of IFN- γ in that particular mouse could be attributed to a potential human error in administration or testing, or it could be indicative of other, unknown immunosuppressive factors at play that have not been tested for.

As expected, none of the treated mice exhibited any significant IL-10 production. Naturally, this is because they did not have established tumors, which typically lead to the overproduction of this cytokine. In contrast, mice injected with RENCA-CRL 2947 cells generated notable amounts of IL-10 as anticipated. These results align with the existing literature regarding the pathways of IL-10 production by tumor cells [19, 21, 22, 65].

The data concerning metastasis occurrence also align with our expected trends. Naturally, we anticipated a higher frequency of metastasis in the untreated group. As previously mentioned, RENCA CRL-2947 typically doesn't exhibit early metastasis, but once the primary tumor

reaches a critical, life-threatening size, metastasis becomes inevitable. Notably, the treatment substances not only reduced tumor growth in some instances but also reduced the occurrence of metastasis. Treated tumors displayed early demarcation, indicating that these substances reactivated cytotoxic CD8⁺ T-cells and other immune cells, leading to a distinct border between the tumor and surrounding tissue. In contrast, untreated tumors rapidly underwent necrosis and lacked these well-defined boundaries. Although the treatment substances couldn't entirely eliminate metastasis, they did visibly reduce its occurrence, which is a promising outcome.

Ultimately, although not all our results were flawless, strong patterns emerged when comparing our treated mice to the control groups. Some discrepancies in the data could be attributed to human errors during animal handling and testing. Additionally, it is important to acknowledge that while the pathways of immune activation via each treatment substance have been described in literature, there may be unreported *in vivo* factors that could be disrupting these pathways. Nevertheless, in light of our findings, we consider these treatments as a robust foundation for future exploration in immunotherapeutic studies. As of October 2023, no studies have investigated the combined effects of RIG-I ligands and anti-OX40 as co-stimulants, nor have they explored the impact of all three immunostimulants together, to the best of the author's knowledge. Moreover, adjusting treatment concentrations and frequencies may yield even more significant results in the examined data, provided these combinations are thoroughly assessed for cytotoxicity levels before human or animal trials. Finding these ideal combinations may eventually address issues related to primary and acquired resistance as well as metastasis, particularly when integrated with other oncotherapies. Further investigations into these variables hold potential for promising discoveries on the frontiers of cancer research.

6. Abstracts

6.1 English Abstract

For many years, it has been understood that the immune system can eliminate developing tumors. However, immunosuppressive factors expressed by malignant cells may impede the host's ability to eradicate established tumors by disrupting the balance between regulatory and effector immune cells. Thus, finding the right combination of immunostimulants has been at the forefront of immuno-oncology research in recent years.

Cytosine-phosphorothioate-Guanine oligodeoxynucleotide (CpG ODN) is a biopolymer that has exhibited promising results in murine models, leading to the regression of specific tumors when administered alongside an anti-OX40 antibody. This therapeutic synergy has demonstrated the ability to reactivate cytotoxic immune cells, ultimately leading to eradication of the targeted tumors. However, these effects have received limited characterization in the context of tumors exhibiting high heterogeneity or low antigen presentation, such as the highly aggressive renal carcinoma cell line RENCA CRL-2947. Additionally, these low molecular weight substances may prove cytotoxic when administered in high concentrations, thus the antitumor effect of a retinoic acid-inducible gene I (RIG-I) ligand was concurrently examined due to its low cytotoxicity index.

In this experiment, we explored the effects of different treatments on renal carcinomas. Specifically, we investigated three treatment groups: Group 1 received CpG ODN and anti-OX40, Group 2 received a combination of CpG ODN with the RIG-I ligand, and Group 3 received the RIG-I ligand as a monotherapy. We inoculated 40 BALB/c mice with the RENCA CRL-2947 cell line and administered each treatment to the corresponding group of mice. Treatments were injected on days 10, 14, and 17 after implantation. We closely monitored these groups, assessing factors including median survival time, average tumor size, cytokine production, and metastatic reduction, all in comparison to an untreated control group.

Our results show that groups 1 and 3 both had higher median survival times compared to the control group. However, groups 1 and 2 were the only two to show a significant reduction in tumor growth after day 24. All three groups exhibited reduced occurrence of metastasis compared to the control, and proinflammatory cytokines were produced in nearly all examined treatment groups.

These data provide a promising foundation for adjusting treatment combinations and frequencies in future studies on renal carcinomas, and offer insights into the potential applications of immunotherapy, particularly when coupled with other oncotherapies.

6.2 Hungarian Abstract

Évek óta tudjuk, hogy az immunrendszer képes fejlődő daganatokat eltávolítani. Azonban a malignus sejtek által kifejezett immunszuppresszív tényezők zavarhatják a test képességét a kialakult daganatok eltávolításában a szabályozó és ható immunitás közötti egyensúly felborításával. Így az immunstimulánsok megfelelő kombinációjának megtalálása az immunológiai kutatások élénk területe lett az utóbbi években.

A citozin-foszforotioát-guanin oligodeoxinukleotid (CpG ODN) egy olyan biopolimer, amely ígéretes eredményeket mutatott egérmodellekben, különösen bizonyos daganatok visszaszorításában, amikor egy anti-OX40 ellenanyaggal együtt adták be. Ez a terápiás szinergia képes volt újraaktiválni a citotoxikus immunsejteket, végül a céldaganatok eltávolításához vezetett. Azonban ezeket az hatásokat korlátozottan jellemzik a nagy heterogenitást vagy alacsony antigénprezentációt mutató daganatok kontextusában, például a magas agresszivitású vese carcinoma sejtvonalban, a RENCA CRL-2947-ben. Ezen kívül ezek a kis molekulatömegű anyagok citotoxikusnak bizonyulhatnak, ha nagy koncentrációban adják be. Ezért a retinsav-indukálható gén I (RIG-I) ligand antitumor hatását is vizsgáltuk, mivel alacsony citotoxicitási indexsel rendelkezik.

Ebben a kísérletben különböző kezelések hatásait vizsgáltuk vese daganatokon. Konkrétan három kezelési csoportot vizsgáltunk: Az 1. csoport CpG ODN-t és anti-OX40-et kapott, a 2. csoport CpG ODN és RIG-I ligand kombinációját, a 3. csoport pedig a RIG-I ligandot kapta monoterápiaként. 40 BALB/c egeret oltottunk be a RENCA CRL-2947 sejtvonallal, és mindegyik csoportnak megfelelő kezelést adtunk. A kezeléseket az implantáció utáni 10., 14. és 17. napon végeztük. Figyelemmel kísértük ezeket a csoportokat, és értékeltük azokat a tényezőket, beleértve a medián túlélési időt, az átlagos daganatméretet, a citokintermelést és a metasztatikus csökkenést, mindezt összehasonlítva az el kezeletlen kontrollcsoporttal.

Az eredményeink azt mutatják, hogy az 1. és a 3. csoportnak magasabb medián túlélési ideje volt, mint a kontrollcsoportnak. Azonban az 1. és a 2. csoport egyedei voltak az egyetlenek, akik jelentős tumorcsökkenést mutattak a 24. nap után. Mindhárom csoportban csökkent a

metasztázis előfordulása a kontrollhoz képest, és a vizsgált kezelési csoportok közül majdnem mindegyikben progyulladásos citokinek voltak jelen.

Ezek az adatok ígéretes alapot nyújtanak a későbbi vizsgálatok során a vese daganatok kezelési gyakoriságának és kombinációinak módosításához, és bepillantást nyújtanak az immunterápia potenciális alkalmazásába.

7. Reference List

1. Mokhtari RB, Sambhi M, Qorri B, Baluch N, Ashayeri N, Kumar S, Cheng H-LM, Yeager H, Das B, Szwczuk MR (2021) The Next-Generation of Combination Cancer Immunotherapy: Epigenetic Immunomodulators Transmogrify Immune Training to Enhance Immunotherapy. *Cancers (Basel)* 13:3596. <https://doi.org/10.3390/cancers13143596>
2. Charles A Janeway J, Travers P, Walport M, Shlomchik MJ (2001) The production of armed effector T cells. In: *Immunobiology: The Immune System in Health and Disease*. 5th edition. Garland Science
3. Laidlaw BJ, Craft J, Kaech SM (2016) The multifaceted role of CD4⁺ T cells in the regulation of CD8⁺ T cell memory maturation. *Nat Rev Immunol* 16:102–111. <https://doi.org/10.1038/nri.2015.10>
4. Ledbetter JA, Linsley PS (1998) CD28. In: Delves PJ (ed) *Encyclopedia of Immunology (Second Edition)*. Elsevier, Oxford, pp 482–483
5. O'Neill RE, Cao X (2019) Chapter Three - Co-stimulatory and co-inhibitory pathways in cancer immunotherapy. In: Wang X-Y, Fisher PB (eds) *Advances in Cancer Research*. Academic Press, pp 145–194
6. Fuse S, Obar JJ, Bellfy S, Leung EK, Zhang W, Usherwood EJ (2006) CD80 and CD86 Control Antiviral CD8⁺ T-Cell Function and Immune Surveillance of Murine Gammaherpesvirus 68. *J Virol* 80:9159–9170. <https://doi.org/10.1128/JVI.00422-06>
7. Alves Costa Silva C, Facchinetti F, Routy B, Derosa L (2020) New pathways in immune stimulation: targeting OX40. *ESMO Open* 5:e000573. <https://doi.org/10.1136/esmoopen-2019-000573>
8. Wajant H, Pfizenmaier K, Scheurich P (2003) Tumor necrosis factor signaling. *Cell Death Differ* 10:45–65. <https://doi.org/10.1038/sj.cdd.4401189>
9. Bourgeois C, Rocha B, Tanchot C (2002) A role for CD40 expression on CD8⁺ T cells in the generation of CD8⁺ T cell memory. *Science* 297:2060–2063. <https://doi.org/10.1126/science.1072615>
10. Zloza A, Kohlhapp FJ, Lyons GE, Schenkel JM, Moore TV, Lacey AT, O'Sullivan JA, Varanasi V, Williams JW, Jagoda MC, Bellavance EC, Marzo AL, Thomas PG, Zafirova B, Polić B, Al-Harhi L, Sperling AI, Guevara-Patiño JA (2012) NKG2D signaling on CD8⁺ T cells represses T-bet and rescues CD4-unhelped CD8⁺ T cell memory recall but not effector responses. *Nat Med* 18:422–428. <https://doi.org/10.1038/nm.2683>
11. Janssen EM, Lemmens EE, Wolfe T, Christen U, von Herrath MG, Schoenberger SP (2003) CD4⁺ T cells are required for secondary expansion and memory in CD8⁺ T lymphocytes. *Nature* 421:852–856. <https://doi.org/10.1038/nature01441>
12. Thaiss C, Semmling V, Franken L, Wagner H, Kurts C (2011) Chemokines: A New Dendritic Cell Signal for T Cell Activation. *Frontiers in Immunology* 2:
13. Romagnani S (1999) Th1/Th2 cells. *Inflamm Bowel Dis* 5:285–294. <https://doi.org/10.1097/00054725-199911000-00009>
14. Constant SL, Bottomly K (1997) Induction of Th1 and Th2 CD4⁺ T cell responses: the alternative approaches. *Annu Rev Immunol* 15:297–322. <https://doi.org/10.1146/annurev.immunol.15.1.297>
15. Filén S, Lahesmaa R (2010) GIMAP proteins in T-lymphocytes. *Journal of signal transduction* 2010:268589. <https://doi.org/10.1155/2010/268589>
16. Li X, Zheng Y (2015) Regulatory T cell identity: formation and maintenance. *Trends Immunol* 36:344–353. <https://doi.org/10.1016/j.it.2015.04.006>
17. Tauriello DVF, Sancho E, Batlle E (2022) Overcoming TGFβ-mediated immune evasion in cancer. *Nat Rev Cancer* 22:25–44. <https://doi.org/10.1038/s41568-021-00413-6>
18. Li MO, Flavell RA (2008) Contextual Regulation of Inflammation: A Duet by Transforming Growth Factor-β and Interleukin-10. *Immunity* 28:468–476. <https://doi.org/10.1016/j.immuni.2008.03.003>
19. Trinchieri G (2007) Interleukin-10 production by effector T cells: Th1 cells show self control. *Journal of Experimental Medicine* 204:239–243. <https://doi.org/10.1084/jem.20070104>
20. Batlle E, Massagué J (2019) Transforming Growth Factor-β Signaling in Immunity and Cancer. *Immunity* 50:924–940. <https://doi.org/10.1016/j.immuni.2019.03.024>
21. González-Garza M, Cruz-Vega D, Bernal C (2020) IL10 as Cancer Biomarker
22. Dennis KL, Blatner NR, Gounari F, Khazaie K (2013) Current status of interleukin-10 and regulatory T-cells in cancer. *Current Opinion in Oncology* 25:637. <https://doi.org/10.1097/CCO.0000000000000006>
23. Contardi E, Palmisano GL, Tazzari PL, Martelli AM, Falà F, Fabbri M, Kato T, Lucarelli E, Donati D, Polito L, Bolognesi A, Ricci F, Salvi S, Gargaglione V, Mantero S, Alberghini M, Ferrara GB, Pistillo MP (2005) CTLA-4 is constitutively expressed on tumor cells and can trigger apoptosis upon ligand interaction. *Int J Cancer* 117:538–550. <https://doi.org/10.1002/ijc.21155>

24. Smyth M, Ngiow S, Teng M (2014) Targeting regulatory T cells in tumor immunotherapy. *Immunology and cell biology* 92:. <https://doi.org/10.1038/icb.2014.33>
25. Wittke S, Baxmann S, Fahlenkamp D, Kiessig ST (2016) Tumor heterogeneity as a rationale for a multi-epitope approach in an autologous renal cell cancer tumor vaccine. *OncoTargets and Therapy* 9:523–537. <https://doi.org/10.2147/OTT.S92182>
26. Aspeslagh S, Postel-Vinay S, Rusakiewicz S, Soria J-C, Zitvogel L, Marabelle A (2016) Rationale for anti-OX40 cancer immunotherapy. *Eur J Cancer* 52:50–66. <https://doi.org/10.1016/j.ejca.2015.08.021>
27. Zhou Z, Lin L, An Y, Zhan M, Chen Y, Cai M, Zhu X, Lu L, Zhu K (2021) The Combination Immunotherapy of TLR9 Agonist and OX40 Agonist via Intratumoural Injection for Hepatocellular Carcinoma. *J Hepatocell Carcinoma* 8:529–543. <https://doi.org/10.2147/JHC.S301375>
28. Sagiv Barfi I, Czerwinski DK, Shree T, Levy R (2018) In Situ Vaccination with CpG and Anti-OX40 Antibody: Preclinical Optimization for Clinical Translation. *Blood* 132:2943. <https://doi.org/10.1182/blood-2018-99-117872>
29. Pieper AA, Spiegelman DV, Felder MAR, Feils AS, Tsarovsky NW, Zaborek J, Morris ZS, Erbe AK, Rakhmilevich AL, Sondel PM (2023) Factors impacting the efficacy of the in-situ vaccine with CpG and OX40 agonist. *Cancer Immunol Immunother* 72:2459–2471. <https://doi.org/10.1007/s00262-023-03433-3>
30. Sagiv-Barfi I, Czerwinski DK, Levy S, Alam IS, Mayer AT, Gambhir SS, Levy R (2018) Eradication of spontaneous malignancy by local immunotherapy. *Sci Transl Med* 10:eaan4488. <https://doi.org/10.1126/scitranslmed.aan4488>
31. Jensen SM, Maston LD, Gough MJ, Ruby CE, Redmond WL, Crittenden M, Li Y, Puri S, Poehlein CH, Morris N, Kovacovics-Bankowski M, Moudgil T, Twitty C, Walker EB, Hu H-M, Urba WJ, Weinberg AD, Curti BD, Fox BA (2010) Signaling through OX40 Enhances Anti-tumor Immunity. *Semin Oncol* 37:524–532. <https://doi.org/10.1053/j.seminoncol.2010.09.013>
32. Deng J, Zhao S, Zhang X, Jia K, Wang H, Zhou C, He Y (2019) OX40 (CD134) and OX40 ligand, important immune checkpoints in cancer. *Onco Targets Ther* 12:7347–7353. <https://doi.org/10.2147/OTT.S214211>
33. Moran AE, Polesso F, Weinberg AD (2016) Immunotherapy Expands and Maintains the Function of High-Affinity Tumor-Infiltrating CD8 T Cells In Situ. *J Immunol* 197:2509–2521. <https://doi.org/10.4049/jimmunol.1502659>
34. Redmond WL, Linch SN, Kasiewicz MJ (2014) Combined targeting of costimulatory (OX40) and coinhibitory (CTLA-4) pathways elicits potent effector T cells capable of driving robust antitumor immunity. *Cancer Immunol Res* 2:142–153. <https://doi.org/10.1158/2326-6066.CIR-13-0031-T>
35. Zhang X, Xiao X, Lan P, Li J, Dou Y, Chen W, Ishii N, Chen S, Xia B, Chen K, Taparowsky E, Li XC (2018) OX40 Costimulation Inhibits Foxp3 Expression and Treg Induction via BATF3-Dependent and Independent Mechanisms. *Cell Reports* 24:607–618. <https://doi.org/10.1016/j.celrep.2018.06.052>
36. So T, Croft M (2007) Cutting edge: OX40 inhibits TGF-beta- and antigen-driven conversion of naive CD4 T cells into CD25+Foxp3+ T cells. *J Immunol* 179:1427–1430. <https://doi.org/10.4049/jimmunol.179.3.1427>
37. TLR9 toll like receptor 9 [Homo sapiens (human)] - Gene - NCBI. <https://www.ncbi.nlm.nih.gov/gene?Db=gene&Cmd=ShowDetailView&TermToSearch=54106>. Accessed 15 Sep 2023
38. Offermanns S, Rosenthal W (2008) *Encyclopedia of Molecular Pharmacology*. Springer Science & Business Media
39. Matz KM, Guzman RM, Goodman AG (2019) Chapter Two - The Role of Nucleic Acid Sensing in Controlling Microbial and Autoimmune Disorders. In: Vanpouille-Box C, Galluzzi L (eds) *International Review of Cell and Molecular Biology*. Academic Press, pp 35–136
40. Sun Y, Reddy P (2013) CH 18 - Intracellular sensors of immunity and allogeneic hematopoietic stem cell transplantation. In: Socié G, Blazar BR (eds) *Immune Biology of Allogeneic Hematopoietic Stem Cell Transplantation*. Academic Press, San Diego, pp 425–447
41. Noh J-Y, Yoon SR, Kim T-D, Choi I, Jung H (2020) Toll-Like Receptors in Natural Killer Cells and Their Application for Immunotherapy. *J Immunol Res* 2020:2045860. <https://doi.org/10.1155/2020/2045860>
42. Marshall JD, Heeke DS, Abbate C, Yee P, Van Nest G (2006) Induction of interferon- γ from natural killer cells by immunostimulatory CpG DNA is mediated through plasmacytoid-dendritic-cell-produced interferon- α and tumour necrosis factor- α . *Immunology* 117:38–46. <https://doi.org/10.1111/j.1365-2567.2005.02261.x>
43. Li T, Wu J, Zhu S, Zang G, Li S, Lv X, Yue W, Qiao Y, Cui J, Shao Y, Zhang J, Liu Y-J, Chen J (2020) A Novel C Type CpG Oligodeoxynucleotide Exhibits Immunostimulatory Activity In Vitro and Enhances Antitumor Effect In Vivo. *Frontiers in Pharmacology* 11:

44. Krieg AM (2002) CpG Motifs in Bacterial DNA and Their Immune Effects. *Annual Review of Immunology* 20:709–760. <https://doi.org/10.1146/annurev.immunol.20.100301.064842>
45. Proskurina AS, Ruzanova VS, Ritter GS, Efremov YR, Mustafin ZS, Lashin SA, Burakova EA, Fokina AA, Zatsepin TS, Stetsenko DA, Leplina OY, Ostanin AA, Chernykh ER, Bogachev SS (2022) Antitumor efficacy of multi-target in situ vaccinations with CpG oligodeoxynucleotides, anti-OX40, anti-PD1 antibodies, and aptamers. *J Biomed Res* 37:194–212. <https://doi.org/10.7555/JBR.36.20220052>
46. Hong WX, Sagiv-Barfi I, Czerwinski DK, Sallets A, Levy R (2022) Neoadjuvant Intratumoral Immunotherapy with TLR9 Activation and Anti-OX40 Antibody Eradicates Metastatic Cancer. *Cancer Res* 82:1396–1408. <https://doi.org/10.1158/0008-5472.CAN-21-1382>
47. Rehwinkel J, Gack MU (2020) RIG-I-like receptors: their regulation and roles in RNA sensing. *Nat Rev Immunol* 20:537–551. <https://doi.org/10.1038/s41577-020-0288-3>
48. Kato H, Takeuchi O, Mikamo-Satoh E, Hirai R, Kawai T, Matsushita K, Hiiragi A, Dermody TS, Fujita T, Akira S (2008) Length-dependent recognition of double-stranded ribonucleic acids by retinoic acid-inducible gene-I and melanoma differentiation-associated gene 5. *J Exp Med* 205:1601–1610. <https://doi.org/10.1084/jem.20080091>
49. Zeng W, Sun L, Jiang X, Chen X, Hou F, Adhikari A, Xu M, Chen ZJ (2010) Reconstitution of the RIG-I pathway reveals a signaling role of unanchored polyubiquitin chains in innate immunity. *Cell* 141:315–330. <https://doi.org/10.1016/j.cell.2010.03.029>
50. Borg N (2019) RIG-I like receptors. *WikiJournal of Science* 2:1. <https://doi.org/10.15347/WJS/2019.001>
51. Berke IC, Modis Y (2012) MDA5 cooperatively forms dimers and ATP-sensitive filaments upon binding double-stranded RNA. *EMBO J* 31:1714–1726. <https://doi.org/10.1038/emboj.2012.19>
52. Levy DE, Marié IJ, Durbin JE (2011) Induction and Function of Type I and III Interferon in Response to Viral Infection. *Curr Opin Virol* 1:476–486. <https://doi.org/10.1016/j.coviro.2011.11.001>
53. Hermant P, Michiels T (2014) Interferon- λ in the Context of Viral Infections: Production, Response and Therapeutic Implications. *J Innate Immun* 6:563–574. <https://doi.org/10.1159/000360084>
54. Tau G, Rothman P (1999) Biologic functions of the IFN- γ receptors. *Allergy* 54:1233–1251. <https://doi.org/10.1034/j.1398-9995.1999.00099.x>
55. Morinobu A, Gadina M, Strober W, Visconti R, Fornace A, Montagna C, Feldman GM, Nishikomori R, O’Shea JJ (2002) STAT4 serine phosphorylation is critical for IL-12-induced IFN- γ production but not for cell proliferation. *Proc Natl Acad Sci U S A* 99:12281–12286. <https://doi.org/10.1073/pnas.182618999>
56. Bhat MY, Solanki HS, Advani J, Khan AA, Keshava Prasad TS, Gowda H, Thiagarajan S, Chatterjee A (2018) Comprehensive network map of interferon gamma signaling. *J Cell Commun Signal* 12:745–751. <https://doi.org/10.1007/s12079-018-0486-y>
57. Hamza T, Barnett J, Li B (2010) Interleukin 12 a Key Immunoregulatory Cytokine in Infection Applications. *International journal of molecular sciences* 11:789–806. <https://doi.org/10.3390/ijms11030789>
58. Tanaka T, Narazaki M, Kishimoto T (2014) IL-6 in Inflammation, Immunity, and Disease. *Cold Spring Harb Perspect Biol* 6:a016295. <https://doi.org/10.1101/cshperspect.a016295>
59. Kishimoto T (1989) The biology of interleukin-6. *Blood* 74:1–10
60. Choy E, Rose-John S (2017) Interleukin-6 as a Multifunctional Regulator: Inflammation, Immune Response, and Fibrosis. *Journal of Scleroderma and Related Disorders* 2:S1–S5. <https://doi.org/10.5301/jsrd.5000265>
61. Renca Syngeneic Murine Model. In: Altogen Labs. <https://altogenlabs.com/xenograft-models/kidney-cancer-xenograft/renca-xenograft-model/>. Accessed 21 Sep 2023
62. Cairns P (2011) Renal Cell Carcinoma. *Cancer Biomark* 9:461–473. <https://doi.org/10.3233/CBM-2011-0176>
63. Kálfalvy-Molnár L, Gulyás D, Lőrincz M (2021) Effects of natural immune response modification on survival of renal carcinoma cells implanted in mice
64. Cannibalism in Laboratory Rodents: Stressors to Avoid. <https://www.clearh2o.com/2021/06/01/cannibalism-in-laboratory-rodents-stressors-to-avoid/>. Accessed 7 Oct 2023
65. Said EA, Dupuy FP, Trautmann L, Zhang Y, Shi Y, El-Far M, Hill BJ, Noto A, Ancuta P, Peretz Y, Fonseca SG, Van Grevenynghe J, Boulassel MR, Bruneau J, Shoukry NH, Routy J-P, Douek DC, Haddad EK, Sekaly R-P (2010) Programmed death-1-induced interleukin-10 production by monocytes impairs CD4+ T cell activation during HIV infection. *Nat Med* 16:452–459. <https://doi.org/10.1038/nm.2106>

8. Figures List

Figure 1-1: Showcasing the four categories of immunotherapy. From left to right: Cancer Vaccines, Checkpoint Inhibitors (ICBs), Chimeric antigen receptor (CAR) T-cell therapy, and Cytokines. Picture adapted from Mokhtari RB, Sambi M, Qorri B, Baluch N, Ashayeri N, Kumar S, Cheng H-LM, Yeger H, Das B, Szewczuk MR (2021) The Next-Generation of Combination Cancer Immunotherapy: Epigenetic Immunomodulators Transmogrify Immune Training to Enhance Immunotherapy. *Cancers (Basel)* 13:3596.

Figure 1-2: A visual representation of various sub-groups found in differentiated T-cells. **Thp** – Naïve T-cells. **IL** – Interleukin. **TGF- β** – Transforming Growth Factor Beta. **Th1** – Type 1 helper T-cell. **Th2** – Type 2 helper T-cell. **Th17** – Type 17 Helper T-cell. **Treg** – Regulatory T-cell. Picture adapted from Filén S, Lahesmaa R (2010) GIMAP proteins in T-lymphocytes. *Journal of signal transduction* 2010:268589.

Figure 1-3: Basic mechanism of OX40 and OX40 Ligand (OX40L) as part of the T-cell activation pathway through major histocompatibility complexes (MHCs) present on myeloid dendritic cells. Anti-OX40 directly boosts expansion and function of effector T-cells, while simultaneously blocking the suppressive effects of regulatory T-cells (Tregs). This leads to a two-fold stimulation of effector T-cells. Picture adapted from Alves Costa Silva C, Facchinetti F, Routy B, Derosa L (2020) New pathways in immune stimulation: targeting OX40. *ESMO Open* 5:e000573.

Figure 1-4: IFN induction pathway as signaled by RIG-I binding to viral RNA. RIG-I binding to RNA allows MAVS recruitment of factors TRAF3, TNK1, and IKK ϵ , leading to subsequent activation of IRF3 or IRF7. Finally, transcription factor binding to nuclear DNA allows IFN production. ‘Ub’ refers to a polyubiquitin chain, used to help viral RNA expose the RIG-I CARD, ‘P’ refers to phosphorylation of the Interferon Regulatory Factor (IRF)3/7. Picture adapted from Borg N (2019) RIG-I like receptors. *WikiJournal of Science* 2:1. 10.15347/WJS/2019.001

Figure 1-5: Positive feedback loop of IL-12 and IFN γ . The loop begins with IL-12 bound to p40 and p35 subunits. JAK-2, along with tyrosine kinase-2 (Tyk2) will recruit phosphorylated STAT4. The dimer moves into the nucleus to induce IFN γ production. IFN γ in turn activates NK cells, T-cells, and macrophages (represented in straight green arrows). IFN γ induces macrophages in particular to release more IL-12, and the cycle starts anew. Picture adapted from Hamza T, Barnett J, Li B (2010) Interleukin 12 a Key Immunoregulatory Cytokine in Infection Applications. *International journal of molecular sciences* 11:789–806.

Figure 1-6: Three types of interactions between T-helper 1 (Th1) release of Interleukin-10 (IL-10), Interleukin-12 (IL-12), and Interferon γ (IFN γ) in the presence of a parasitic infection. (A) IL-10, IFN γ , and IL-12 are all produced in equal amounts. IL-10 prevents overproduction of IFN γ and IL-12, meaning the three cannot effectively eradicate intracellular parasites (represented by blue flowers). (B) IL-10 and parasites block both IFN γ and IL-12, leading to no inflammatory response and an overpopulation of parasites. (C) IL-10 production is entirely stopped, leading to overproduction of IFN γ and IL-12. This eliminates the parasites but can damage surrounding tissue. Picture adapted from Trinchieri G (2007) Interleukin-10 production by effector T cells: Th1 cells show self control. *Journal of Experimental Medicine* 204:239–243.

Figure 4-1: Survival times of total 40 mice over the course of 40 days. Percentage of living mice is represented as a function of surviving mice (%) over days since tumor implantation. Group one (CpG and antiOX40) is shown in blue, group two (CpG and RIG-I Ligand - 3p-hpRNA) shown in orange, group three (RIG-I Ligand - 3p-hp-RNA) shown in purple, and the untreated PBS control group shown in red. Treatments are represented by cyan dashed lines, and were administered on days 10, 14, and 17. Graph by Gulyás Dominik Ádám, Department of Microbiology and Infectious Diseases.

Figure 4-2: Primary tumor growth as shown as a function of size over time. Group one (CpG and antiOX40), shown in blue, group two (CpG and RIG-I Ligand - 3p-hpRNA) shown in orange, group three (RIG-I Ligand - 3p-hp-RNA) shown in purple, and the untreated PBS control group shown in red. Days where all tumors were measured are shown in dotted cyan lines, and were taken on days 17, 24, 31, and 38. Graph by Gulyás Dominik Ádám, Department of Microbiology and Infectious Diseases.

Figure 4-3: Total Interferon- γ (IFN- γ) production in eight mice. Treatment and tumor presence is noted under each bar along the x-axis. IFN- γ production is presented in picograms per milliliter. Graph by Gulyás Dominik Ádám, Department of Microbiology and Infectious Diseases.

Figure 4-4: Total interleukin-6 (IL-6) production in eight mice. Treatment and tumor presence is noted under each bar along the x-axis. IL-6 production is presented in picograms per milliliter. Graph by Gulyás Dominik Ádám, Department of Microbiology and Infectious Diseases.

Figure 4-5: Total interleukin-10 (IL-10) production in eight mice. Treatment and tumor presence is noted under each bar along the x-axis. IL-10 production is presented in picograms per milliliter. Graph by Gulyás Dominik Ádám, Department of Microbiology and Infectious Diseases.

Figure 4-6: Histological slide of a lung metastasis from RENCA CRL-2497 tumor cells stained with haematoxylin-eosin. Abnormal aggregation of cells can be seen in the lower center of the image, lacking the typical appearance of lung tissue. Image by Gulyás Dominik Ádám, Department of Microbiology and Infectious Diseases.

Figure 4-7: Macroscopic (A) and histological (B) appearance of a typical RENCA CRL-2947 primary tumor. Image 4-7A depicts the primary tumor, well encapsulated in the abdominal cavity of a BALB/c mouse. Abdominal organs have been removed. Image 4-7B notes the presence of Giant cells, Necrosis, Blood vessels, and Divided cells. Images by Rhiannon Rodgers (A) and Gulyás Dominik Ádám (B), Department of Microbiology and Infectious Diseases. Image A taken on 15.04.2023.

Table 4-1: Statistical results of treated groups in comparison to the untreated control. Analysis conducted using Mantel-Cox log-rank tests. Groups are colored in accordance with the lines presented in **Figure 4-1**. (Survival curves comparison). Table by Gulyás Dominik Ádám, Department of Microbiology and Infectious Diseases.

Table 4-2: Statistics: Mann-Whitney test (Treated Groups Compared to Untreated PBS Group) ns. – Not significant. sign. – Significant. Groups are colored in accordance with lines in **Figure 4-2**. Table by Gulyás Dominik Ádám, Department of Microbiology and Infectious Diseases.

Table 4-3: Eight mice tested for total production of three cytokines (IFN- γ , IL-6, IL-10). Mice implanted with 200 microliters of RENCA CRL-2947 are noted in the table as “Tumor +”. Those that were not implanted are marked as “Tumor –”. Table by Gulyás Dominik Ádám, Department of Microbiology and Infectious Diseases.

Table 4-4: Metastatic occurrence in each of the tested groups. Locations of metastasis are noted in each column, with the total number of metastatic events in each group listed in the far-right column. * Disseminated tumor cells found in the body cavity, counted in the total number of metastatic events despite not falling under the definition of traditional metastasis. Table by Gulyás Dominik Ádám, Department of Microbiology and Infectious Diseases.

9. Acknowledgements

First and foremost, I would like to extend my deepest gratitude to my advisors, Dr. Lőrincz Márta and Gulyás Dominik, who accepted me onto this project, answered all of my questions with patience, and allowed me the opportunity to fully realize my love of oncology, immunology, and research as a whole. Nagyon szépen köszönöm!

This TDK would never have been possible without the love, care, and support from my parents as they never failed to support me in my big dreams of becoming a veterinarian. I could not have done it without them. This gratitude also extends to the rest of my family, including my brothers, my uncle, and my wonderful grandmother. Thank you all!

I would also like to extend my thanks to Sierra McCarty for not only proofreading all 39 pages, but for being a wonderful friend to me for 9 years and counting. No doubt I would not have made it out with my sanity intact if not for you.

Thank you to Toni Breuer for giving me excellent advice for formatting, proofreading, and answering all of my constant questions. Thanks Toni!

I would also like to thank the rest of my friends for their support and understanding throughout this whole process. I have many of you to thank in person, but this acknowledgements section can only be so long!

Thank you to the rest of the Microbiology and Infectious Diseases department, as well as staff members of NÉBIH for their constant assistance throughout the course of the experiment. In particular, I would like to extend my gratitude to Dr. Béla Dénes, Dr. István Jankovics, Józsefné Herbák, and Földi Dóra.

Finally, thank you to Katie Commins for working on our respective projects alongside me! Best of luck in your future immunological endeavors.

Project no. RRF-2.3.1-21-2022-00001 has been implemented with the support provided by the Recovery and Resilience Facility (RRF), financed under the National Recovery Fund budget estimate, RRF-2.3.1-21 funding scheme.

Project nr. 2019-1.2.1-Egyetemi-Öko-2019-00010 has been implemented with the support provided by the National Research, Development and Innovation Fund of Hungary, financed under the 2019-1.2.1-Egyetemi-Öko funding scheme.

Témavezetői nyilatkozat TDK dolgozathoz

Alulírott, **Gulyás Dominik Ádám**, mint témavezető nyilatkozom, hogy **Rhiannon Rodgers**, 6. évfolyamos hallgató „**Modification of the Innate Immune Response using Low Molecular Weight Substances and its Effects on Renal Carcinoma Cells in a Mouse Model**” című dolgozatát átolvastam és jóváhagytam, részvételét támogatom az Állatorvostudományi Egyetem 2023. évi Tudományos Diákköri Konferenciáján. Továbbá nyilatkozom, hogy a feltöltött TDK dolgozat plágiumellenőrzésen sikeresen átesett és az esetlegesen feltárt egyezőség az Egyetemi iránymutatásoknak/szabályoknak megfelel.

Budapest, 2023. október 20.

..........

témavezető

Témavezetői nyilatkozat TDK dolgozathoz

Alulírott, **Lőrincz Márta**, mint témavezető nyilatkozom, hogy **Rhiannon Rodgers**, 6. évfolyamos hallgató „**Modification of the Innate Immune Response using Low Molecular Weight Substances and its Effects on Renal Carcinoma Cells in a Mouse Model**” című dolgozatát átolvastam és jóváhagytam, részvételét támogatom az Állatorvostudományi Egyetem 2023. évi Tudományos Diákköri Konferenciáján. Továbbá nyilatkozom, hogy a feltöltött TDK dolgozat plágiumellenőrzésen sikeresen átesett és az esetlegesen feltárt egyezőség az Egyetemi iránymutatásoknak/szabályoknak megfelel.

Budapest, 2023. október 20.

.....*Lőrincz Márta*.....

témavezető



Thesis progress report for veterinary students

Name of student: Rodgers Rhiannon
 Neptun code of the student: 1238E3
 Name and title of the supervisor: Marta Lönnér, Senior Lecturer / Dominik Gulyás, Departmental Engineer
 Department: Department of Microbiology and Infectious Diseases
 Thesis title: Modification of the innate immune response with low molecular weight substances and its effects on renal carcinoma cells in a mouse model

Consultation – 1st semester

	Timing			Topic / Remarks of the supervisor	Signature of the supervisor
	year	month	day		
1.	2023	02	02	Designing experimental plan	<i>conna</i> / <i>[Signature]</i>
2.	2023	03	02	Designing experimental plan	<i>conna</i> / <i>[Signature]</i>
3.	2023	04	25	Execution of toxicity pre-experiment	<i>conna</i> / <i>[Signature]</i>
4.	2023	05	05	Evaluation of the results of toxicity pre-experiment	<i>conna</i> / <i>[Signature]</i>
5.	2023	06	01	Executing animal experiment	<i>conna</i> / <i>[Signature]</i>

Grade achieved at the end of the first semester: Excellent (5)

Consultation – 2nd semester

	Timing			Topic / Remarks of the supervisor	Signature of the supervisor
	year	month	day		
1.	2023	06	05	Executing animal experiment	<i>conna</i> / <i>[Signature]</i>
2.	2023	07	15	Evaluation of the results of animal experiment	<i>conna</i> / <i>[Signature]</i>
3.	2023	09	25	Discussion of thesis content	<i>conna</i> / <i>[Signature]</i>
4.	2023	10	01	Discussion of thesis content	<i>conna</i> / <i>[Signature]</i>



5.	2023	10	10	Discussion of thesis conf	adina / G.S.A
----	------	----	----	---------------------------	---------------

Grade achieved at the end of the second semester: *excellent (5)*

The thesis meets the requirements of the Study and Examination Rules of the University and the Guide to Thesis Writing.

I accept the thesis and found suitable to defence,

adina / G.S.A
signature of the supervisor

Signature of the student:

Signature of the secretary of the department: *Jubube' x nana*

Date of handing the thesis in.....